ABS braking on rough terrain

UNIVERSITEIT VAN PRETORIA
UNIVERSITY OF PRETORIA
YUNIBESITHI YA PRETORIA

Nico André van der Merwe

Submitted in partial fulfilment of the requirements for the degree

Master of Engineering
(Mechanical engineering)

In the Faculty of

Engineering, Built Environment and Information Technology
(EBIT)

At the

University of Pretoria

March 2018

Contents

List of figures

List of tables

List of Symbols

Symbol	*Description*	*Units*
A	Maximum wheel acceleration	m/s^2
a	Acceleration	m/s^2
a_{max}	Wheel acceleration threshold	m/s^2
a_{min}	Wheel deceleration threshold	m/s^2
C	Capacitance	$Farads$
C_1, C_2, C_3, C_4	Shape factors	$Dimensionless$
d	Diameter	m
f	Coefficient of friction	$Dimensionless$
$F_{friction}$	Frictional force	N
F_N	Normal force	N
F_{spring}	Force exerted from spring	N
F_x	Longitudinal force	N
F_y	Lateral force	N
F_z	Vertical force	N
g	Gravity	$Constant\ (9.81 m/s^2)$
I_o	Moment of inertia relative to point O	$kg\ m^4$
I_{pitch}	Pitch inertia	$kg\ m^4$
I_{roll}	Roll inertia	$kg\ m^4$
I_{xx}	Inertia about the x axis	$kg\ m^4$
I_{yaw}	Yaw inertia	$kg\ m^4$
I_{yy}	Inertia about the y axis	$kg\ m^4$

I_{zz}	Inertia about the z axis	$kg\ m^4$
l	Length	m
L_{accel}	Length between where acceleration is measured and where the spring induces a vertical acceleration	m
L_{force}	Length between the pivot point and the point where the force is exerted	m
k	Spring stiffness	N/m
$M\ or\ m$	Mass	kg
M_x	Overturning moment	Nm
M_y	Rolling resistance moment	Nm
M_z	Aligning moment	Nm
p	Brake pressure	Pa
p_a	Applied hydraulic brake pressure	Pa
p_{min}	Minimum brake pressure for ABS activation	Pa
r	Radius	m
r_i	Inner brake pad radius	m
r_o	Outer brake pad radius	m
R	Resistance	$Ohms$
R_{eff}	Effective rolling radius	m
R_d	Deceleration constant	$Dimensionless$
s_{max}	Maximum slip threshold	$Dimensionless$
t	Time	$Seconds$

T	Brake torque	Nm
T_o	Torque rotated around point O	Nm
v	Vehicle speed	m/s
$\dot{v}$	Vehicle deceleration	m/s^2
v_{min}	Minimum vehicle speed for ABS activation	m/s
v_w	Wheel speed	m/s
yf_i	Current filtered signal value	m/s
yf_{i-1}	Previous filtered signal value	m/s
y_i	Unfiltered signal value	m/s
x	Linear displacement	m
$\ddot{x}$	Linear acceleration	m/s^2
x_1, x_2	Displacement amplitudes of consecutive oscillations	m
Greek symbols:		
α	Slip angle	$Degrees$
β	Tuning parameter	$Dimensionless$
δ	Logarithmic decrement	$Dimensionless$
ζ	Damping coefficient	$Dimensionless$
θ	Angle	rad
$\Delta\theta\ (=\theta_2-\theta_1)$	Angle of brake pads	rad
$\ddot{\theta}$	Angular acceleration	rad/s^2
λ	Longitudinal slip	$Dimensionless$
μ	Coefficient of friction	$Dimensionless$
τ	Undamped period	$Seconds$

τ_d	Damped period	$Seconds$
τ_{pulse}	Pulse width	$Seconds$
ω	Wheel rotational velocity	rad/s
ω_n	Natural frequency	Hz

Abbreviations

Abbreviation	*Description*
ABS	Anti-lock Braking System
ADAMS	Automated Dynamic Analysis of Mechanical Systems (Multibody Dynamics Software from MSC)
CAN bus	Controller Area Network bus communication
CG	Centre of Gravity
CV	Constant velocity joint
dSPACE	Digital Signal Processing and Control Engineering
dsPIC	Digital Signal Peripheral Interface Controller
ECU	Electric Control Unit
FTire	Flexible Structure Tire Model
GPS	Global Positioning System
I/O	Input/Output signals
LH	Left Hand side
MABX Ⅱ	Micro Auto Box (dSPACE platform)
MOSFET	Metal Oxide Semi-conductor Field Effect Transistor
PWM	Pulse Width Modulation
RH	Right Hand side
RTI	Real Time Interface
SUV	Sport Utility Vehicle
VDG	Vehicle Dynamics Group (University of Pretoria)
VBOX	Velocity Box (GPS and vehicle dynamics measurement device from RACELOGIC)
WFT	Wheel Force Transducer

Abstract

Anti-lock braking systems (ABS) have revolutionised vehicle safety by providing a mechanism for braking effectively whilst maintaining stability control.

ABS works very well on smooth terrains, where there are little disturbances from the terrain and thus has been wildly adopted on commercial vehicles. The ability of ABS to perform on rough terrains is however deteriorated by the fact that rough terrains cause fluctuations in the wheel speeds and in the loading conditions of the tyre, which negatively affects the ABS algorithm as well as the tyre-terrain interaction. The adoption of ABS on off-road vehicles have been very slow due to these challenges.

This study investigates the performance of ABS on rough terrain through performing experimental and simulated ABS tests using a testing trailer. A MSC ADAMS model of the trailer was built and validated. The ABS tests show good correlation between the tyre forces measured and the forces simulated using an FTire (Flexible Structure Tire Model) model in MSC ADAMS. The ABS algorithm's performance deteriorates significantly due to the oscillation of wheel speeds. The work done in this study paves the way towards future ABS investigation and development using both the experimental and a simulated platform.

Acknowledgements

The student thanks Prof P.S. Els for his guidance throughout this study, Carl Becker for his help in the testing process of this study, Gerhard Vosloo for his assistance in characterising the suspension components and Vidas Zuralaulis for his help in modelling and instrumenting the experimental setup. Lastly I would like to thank my parents and my sister for their continuous love and support.

The student also thanks the European Union's Horizon 2020 research and innovation programme under the Marie Skłodowska-Curie grant agreement No 645736, which helped fund this research.

1. Literature review

To understand ABS (Anti-lock Braking System), the interaction between the tyre and the terrain needs to be understood. The first section of this literature study focusses on the fundamentals of braking. The force generation between the tyre and the terrain is discussed and this follows through to the basic working principles of ABS. ABS control strategies such as the classic Bosch algorithm and as well as modern ABS algorithms are explored and the performance of ABS on rough terrain is discussed based on the literature found.

1.1. Fundamental principles of braking

From a braking perspective, the most important forces acting on a vehicle is the interaction forces between the tyres and the terrain. This interaction governs the braking and handling of a vehicle, and is influenced by the properties of the tyres, properties of the terrain and environmental conditions.

1.1.1. Contact force generation

The tyre contact patch of a tyre is the area of the tyre that is in direct contact with the terrain. There are two main contact mechanisms that exist between the terrain and the tyre. The first is called adhesion. This mechanism operates through the intermolecular bonds between the terrain and the tyre. This is the largest component on dry terrain, however is less effective with wet terrain, which causes the tyre to generate less friction (Gillespie, 1992). The second mechanism is hysteresis which works on the energy loss component during the deformation of the tyre tread (Gillespie, 1992). This mechanism can aid in maintaining sufficient friction contact on wet terrain, provided that the tyres' tread contains high-hysteresis rubber.

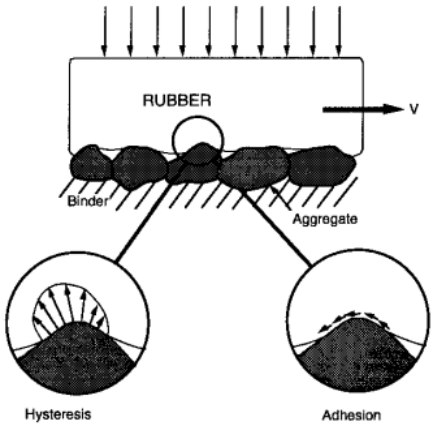

Figure 1: Tyre contact friction generation mechanism
(Gillespie, 1992)

1.1.2. Tyre Force generation

The operation of the tyre is governed by three forces and three moments (Figure 2). An applied wheel torque from either braking or accelerating the tyre is generated.

The forces of the tyre are generated as a result of the external factors acting on the tyre, such as the friction forces that are generated with the tyre-terrain interaction, as well as through the roughness of the terrain. The forces are influenced by internal factors, such as the deformation of the tyre carcass as well as tyre pressure.

The longitudinal force is generated parallel to the direction of the rolling tyre, lateral force is generated normal to the direction of travel of the tyre and vertical force is generated vertically upwards normal to the lateral and longitudinal forces. For each direction of generated force there is an accompanying moment that is also generated along the same direction.

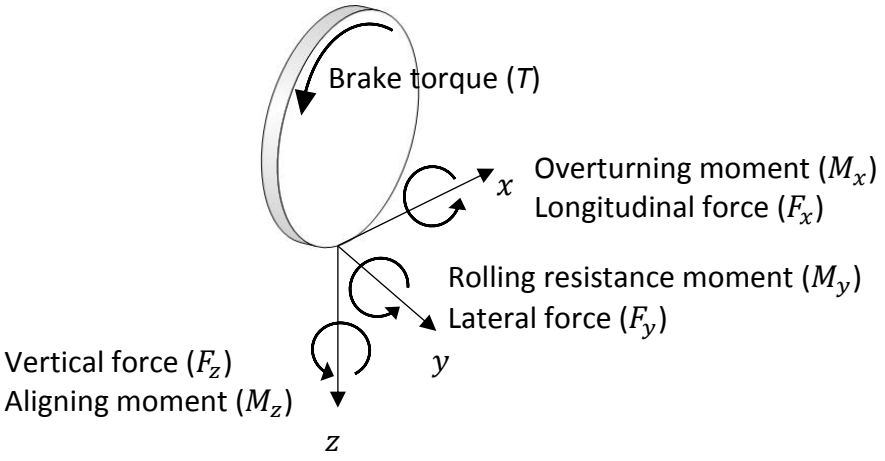

Figure 2: Force and moment generation on a tyre

1.1.3. Vertical force

The vertical force is governed mainly by the internal pressure, carcass stiffness and the damping in the tyre which varies with the deformation of the tyre's carcass. Research shows that the increasing of the vertical load on tyres, decreases the friction coefficient (Gillespie, 1992). The friction coefficients of a tyre (for a particular terrain surface) can decrease by 0.01 for a 10% increase in vertical load (Gillespie, 1992).

1.1.4. Longitudinal force and longitudinal slip

The longitudinal force is generated along the direction of travel of the wheel. This force is generated from the longitudinal frictional force that exists when the wheel is accelerated or braked. This force is affected by the vertical force, the surface friction coefficient (which is dependent on environmental factors), as well as the roughness of the terrain. The longitudinal and vertical deformation of the tyre also plays a role as this affects the magnitude of friction that can be generated.

Longitudinal force is dependent on longitudinal slip (λ). Longitudinal slip is a comparison between the velocity that the vehicle is traveling (v) and the peripheral velocity that the tyre is rolling at. The wheel peripheral velocity is calculated using an effective rolling radius (R_{eff}) of the tyre and through measuring the angular speed of the wheel (ω).

$$\lambda = \frac{v - \omega \cdot R_{eff}}{v} \tag{1}$$

With a rolling tyre, at the leading edge of the tyre contact area, the radius of the tyre reduces from the un-deformed to the deformed radius. There is a change in the velocity of the tyre as it comes into contact with the terrain, due to the reduction in the tyre's radius.

At the trailing edge of the contact patch, the tyre's radius has to increase back to the un-deformed radius as it looses contact with the terrain.

The relative slip therefore changes through the contact patch but usually reaches a peak value slightly behind the centre of the tyre. This varying slip, combined with variations in vertical load and frictional force, governs the longitudinal force generated between the tyre and the terrain.

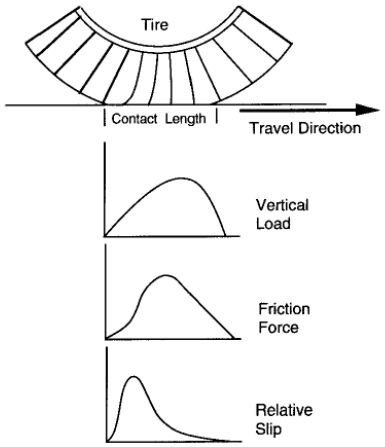

Figure 3: Longitudinal force generation (Gillespie, 1992)

When the tyres are braked, significant longitudinal slip of the tyres can exist. The friction coefficients relative to a specific terrain surface are shown in Figure 4. Wheel lock-up occurs as a result of the wheel slip exceeding the maximum peak friction co-efficient, as the ability of the tyre to generate longitudinal force deteriorates. The wheels lock-up completely at 100% slip, as the wheels are essentially not rotating while the vehicle is still moving.

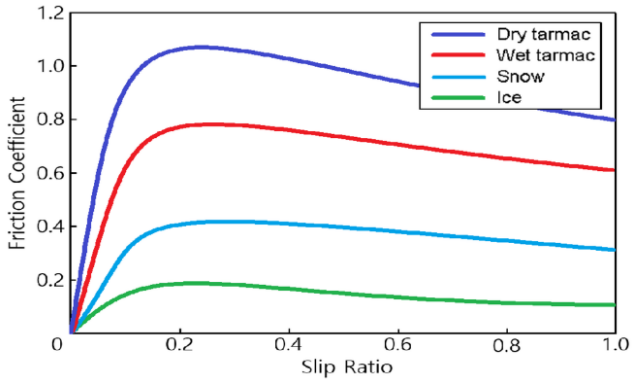

Figure 4: Different friction coefficients for different terrain conditions (Park et al., 2015)

1.1.5. Lateral force and lateral slip

When a vehicle is steered while cornering, lateral force is generated normal to the direction of travel of the wheel. The contact patch of the tyre is manipulated by the direction of travel of the vehicle relative to the direction of heading of the wheel. The difference in the angle is called the slip angle, described with the symbol, α.

The tyre's contact patch remains in line with the direction of travel of the vehicle due to the friction between the tyre and the terrain. The maximum lateral force is generated at an offset from the centre of the tyre. This offset is called the pneumatic trail (Figure 5).

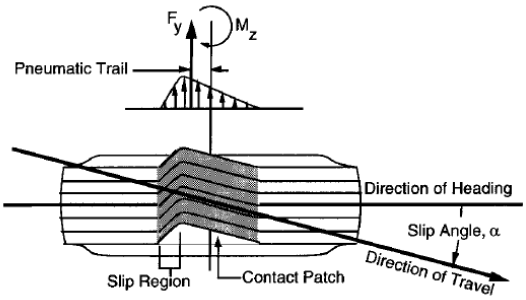

Figure 5: Pneumatic trail of a tyre (Gillespie, 1992)

1.1.6. Combined lateral and longitudinal force generation

Longitudinal and lateral forces are usually generated simultaneously as the vehicle is commonly steered and braked or accelerated at the same time. Longitudinal force generation usually has preference over lateral force generation. Figure 6 shows that, as the longitudinal slip of the tyre increases, the longitudinal force (F_x) also increases to the detriment of the lateral force (F_y), for a given slip angle.

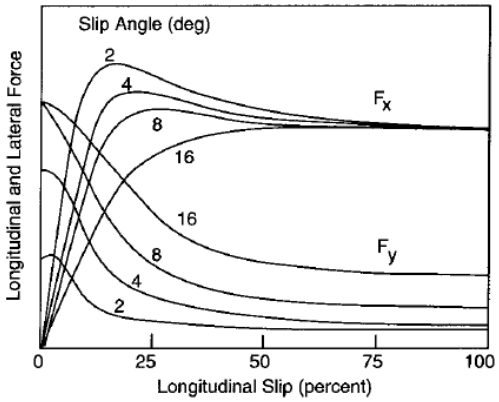

Figure 6: Lateral and Longitudinal force generation versus slip (Gillespie, 1992)

Figure 7 shows a friction circle, which is a diagram that is used to illustrate the friction limit of a tyre for a combination of lateral and longitudinal forces.

The generation of a maximum longitudinal force during either braking or accelerating, does not allow for any lateral force to be generated, and visa versa, otherwise the friction limit of the tyre will be exceeded (fall out of the region of the circle).

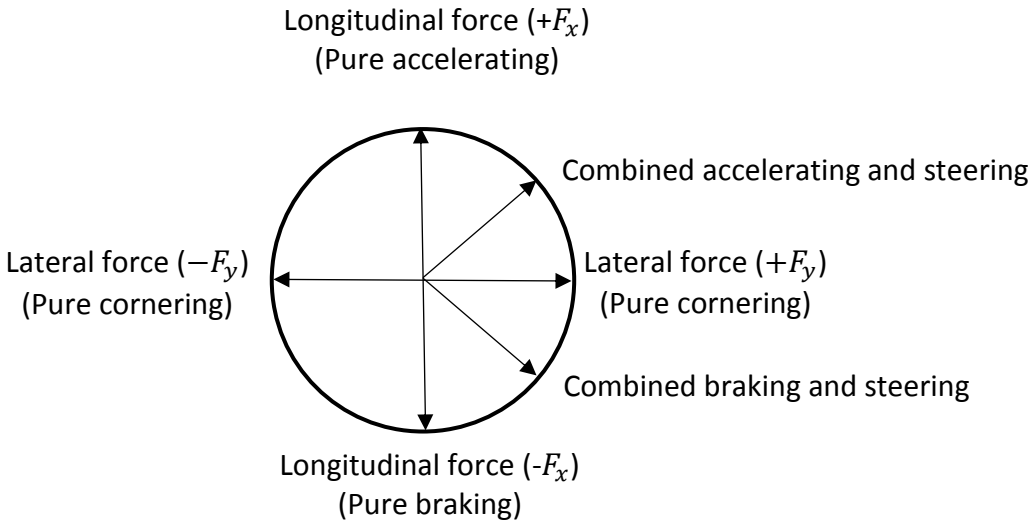

Figure 7: Friction circle

When the maximum friction of the tyre-road contact is exceeded during severe braking, wheel-lock is caused as the brake torque supplied to the wheels is greater than the maximum longitudinal force for a given rolling radius. When wheel lock-up occurs the lateral force is diminished. It is due to this reason that a vehicle is unable to steer when the wheels lock-up.

1.1.7. Hydraulic brake system

A hydraulic brake system is used to control the pressure that is supplied to the brakes of a vehicle. The hydraulic brake lines for a Land Rover Defender is shown in Figure 8 (Rover Group Limited, 1996). This brake system was designed before the introduction of ABS control.

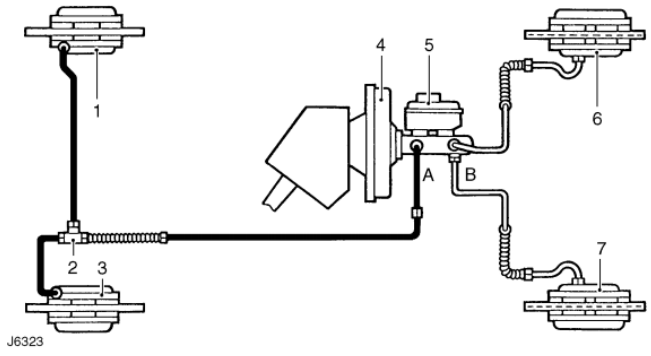

110/130 Models

Hydraulic system

A- Primary circuit
B- Secondary circuit
C- Pressure reducing valve (PRV)

1. LH rear brake caliper
2. T connector
3. RH rear brake caliper
4. Brake servo
5. Master cylinder and reservoir
6. LH front brake caliper
7. RH front brake caliper

Figure 8: Land Rover Defender hydraulic brake line (Rover Group Limited, 1996)

The master cylinder converts the force applied to the brake pedal, to the pressure in the brake lines causing the brake callipers tighten on each wheel's disk brake. A brake booster is also included in within the brake servo (4) setup, which decreases the force required to press the brake pedal through the use of a vacuum pump.

The brake torque of the tyre is generated by friction between the brake pads that press down on brake disks, which are connected to the wheel hubs. The brake pads are fitted around a brake disk through brake callipers, which are connected to the hydraulic brake line and supply the pressure. The friction between the disk brakes (stationary) and the brake drum (rotating) create a braking torque that is experienced by the tyres.

The brake torque (T) is related to the size of the brake pads ($\Delta\theta = \sigma_2 - \sigma_1, r_i \; and \; r_o$), their relative friction coefficient (f), as well as the mean pressure of the brake pads (p_a) seen in equation (2). The brake pad dimension geometry is shown in Figure 9. This relation is based on the assumption that uniform wear of the brake pads is present (Budynas and Nisbett, 2011).

$$T = \frac{1}{3}(\Delta\theta) f p_a (r_0^3 - r_i^3) \tag{2}$$

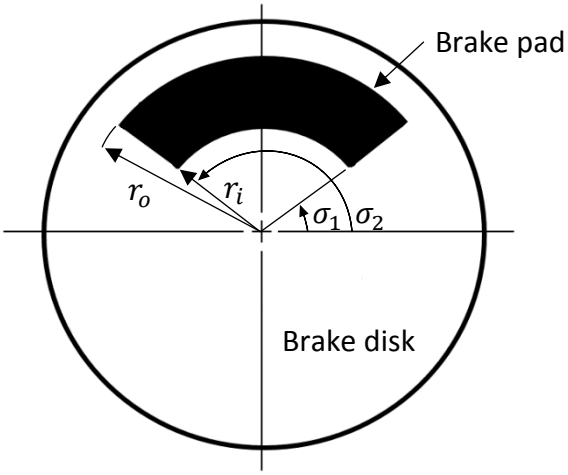

Figure 9: Brake pad geometry

The inclusion of ABS control in the brake system requires a mechanism that can control the brake pressures at each brake calliper independently. An ABS modulator and pump is used to intervene in the control of the brake pressure and is controlled by a vehicle's brake control unit. When ABS is activated, the modulator isolates the brake pressure between the applied pressure from the brake pedal and the existing pressure in the brake lines that flow directly to the brakes. The modulator, with the aid of the pump, will then independently *Pump*, *Dump* or *Hold* the pressure accordingly to what the ABS control requires. Figure 10 shows a simplified hydraulic schematic for an ABS modulator with shuttle valves that isolate the pressure from the brake pedal when ABS is activated. During the *Pump* phase the inlet solenoid valve is open and the outlet solenoid valve is closed. When the modulator is in *Dump* mode, the inlet solenoid valve is open and the outlet solenoid valve is open. The inlet and outlet solenoid valves are closed when the *Hold* phase is activated.

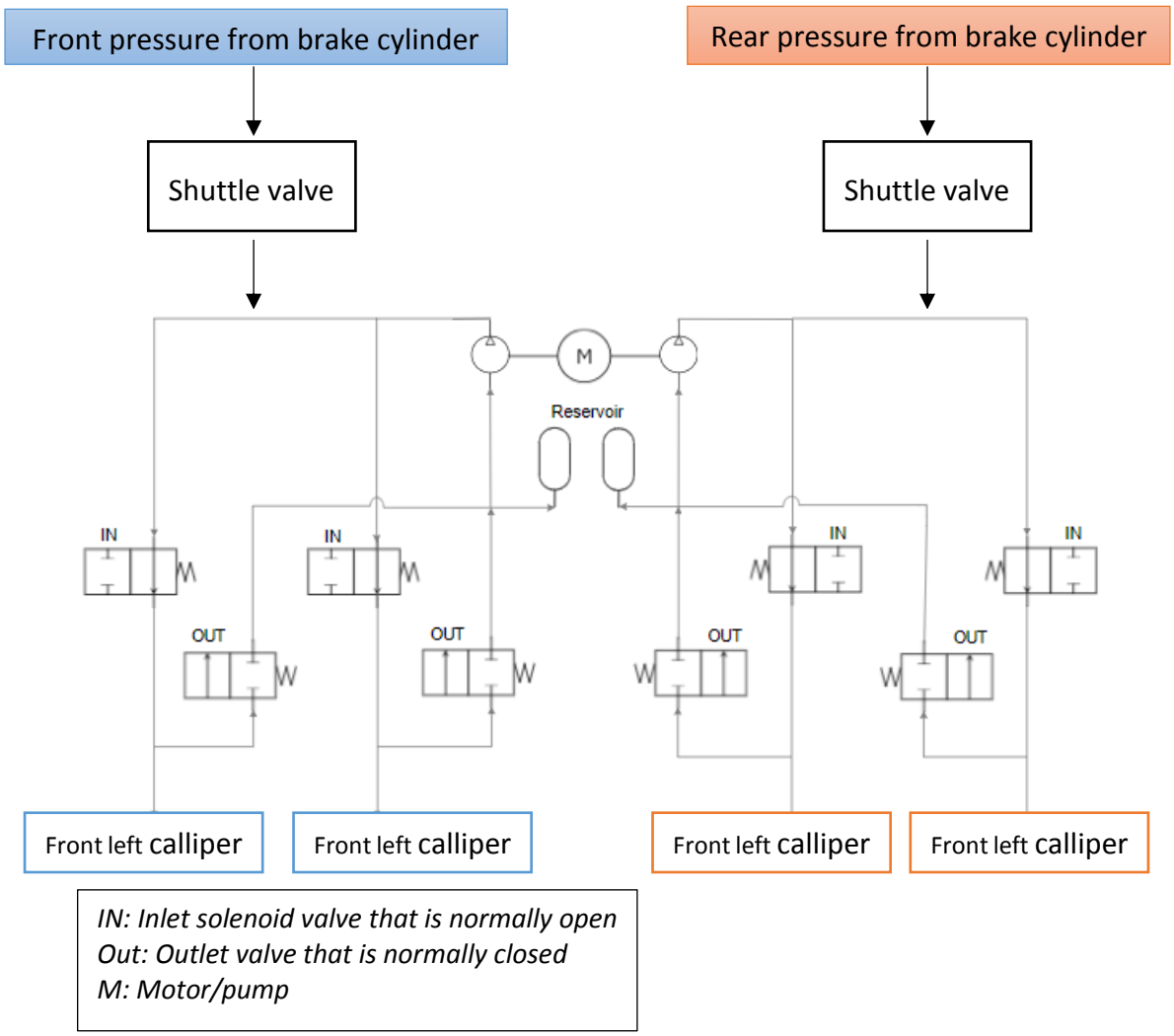

Figure 10: ABS modulator hydraulic schematic

1.1.8. ABS objective

ABS brake systems were first introduced in the early 1970s onto trucks, and made use of high-end electrical components, which were scarce and relatively expensive during that time (Fu, 2000). As the electrical revolution began gaining momentum, electrical components became cheaper to produce and so further advancements in ABS control could take form onto commercials vehicles. During 1978 BOSCH started supplying the first ABS components to commercial vehicle manufactures (SAE Standard, 1992), (Fu, 2000).

The basic aim of an ABS algorithm is to firstly brake the wheel in such a manner as to maintain maximum braking efficiency which occurs when the maximum peak friction coefficient of a tyre is reached without locking the wheel. Secondly, ABS allows the tyres to generate some lateral force for the steer ability of the vehicle while braking.

There are three braking states that an ABS algorithm can use to achieve this. A brake state defines what should be done to the brake pressure of each wheel and can either be defined to increase the pressure (brake state→PUMP), decrease the pressure (brake state→DUMP) or keep the brake pressure constant (brake state→HOLD).

As a force is applied to the brake pedal, in the initial stage of a braking maneuverer, the brake pressure is increased until a preset slip threshold is reached, which coincides with the peak friction of the tyre. Once the slip threshold is reached, ABS sets the brake state to dump (pressure is decreased). The slip of the tyre then falls below the peak friction and the pressure is kept constant once the wheel deceleration reaches a set threshold. This allows the tyre to operate below its maximum peak friction, which allows for some lateral force generation as the friction circle dictates which allows for the vehicle to be steered when being braked. The brake pressure is then increased again to allow the tyre to operate closer to its peak friction. The braking process is repeated and cycled continuously required vehicle speed is achieved. This cycling of brake pressure therefore allows the tyres to operate close to their maximum braking efficiency, while still allowing the generation of some lateral forces for vehicle stability.

1.1.9. Performance evaluation of ABS

The performance evaluation of ABS is usually done through looking at the effective braking distance of a vehicle. This is not always a true evaluation, as ABS should also be evaluated its effectiveness to allowing steering stability. Performance evaluations have been performed taking this into consideration. In an ABS performance evaluation study (Forkenbrock et al., 1999) of nine light commercial vehicles, the ABS performance was evaluated through straight line braking on different friction surfaces, performing J-turns as well as single lane change maneuverers. These maneuverers should be considered if ABS is to be evaluated fully. Furthermore work done by Hamersma and Els (2017), show the importance of collectively considering the stopping distance, the mean deceleration, the mean error of the absolute yaw rate as well as the mean error of the absolute lateral path, for the accurate and logical method of evaluation of ABS performance.

1.1.10. Classic Bosch ABS algorithm

This classic Bosch ABS algorithm requires only the measurement of wheel speeds. From these measurements the wheel angular acceleration can be derived and the longitudinal slip of the tyres can also be calculated. The vehicle speed can be estimated by using the wheel speeds and from this the slip can be approximated.

The classic Bosch ABS algorithm controls the brake pressure through cycling through 8 phases. For each phase a specific brake state is defined. The Bosch algorithm works based on pre-defined wheel accelerations and slip thresholds, that govern the selection of each phase in the algorithm. Suggested values for the Bosch algorithm thresholds are listed in Table 1.

Table 1: Bosch ABS thresholds

Authors	*Minimum wheel acceleration,* $a_{min}\ (rad/s^2)$	*Maximum wheel acceleration,* $a_{max}\ (rad/s^2)$	*Wheel maximum slip,* s_{max}
Day and Roberts (2002)	-150	50	0.15
Penny and Els (2016)	-50	50	0.15

Figure 11 shows the ABS functionality. Each phase has a set duration within which it needs to be operated before it moves onto the next phase (not shown on the diagram). Note that phase 7 is a dual brake state, it oscillates between pump-hold states governed also by specified duration for each state.

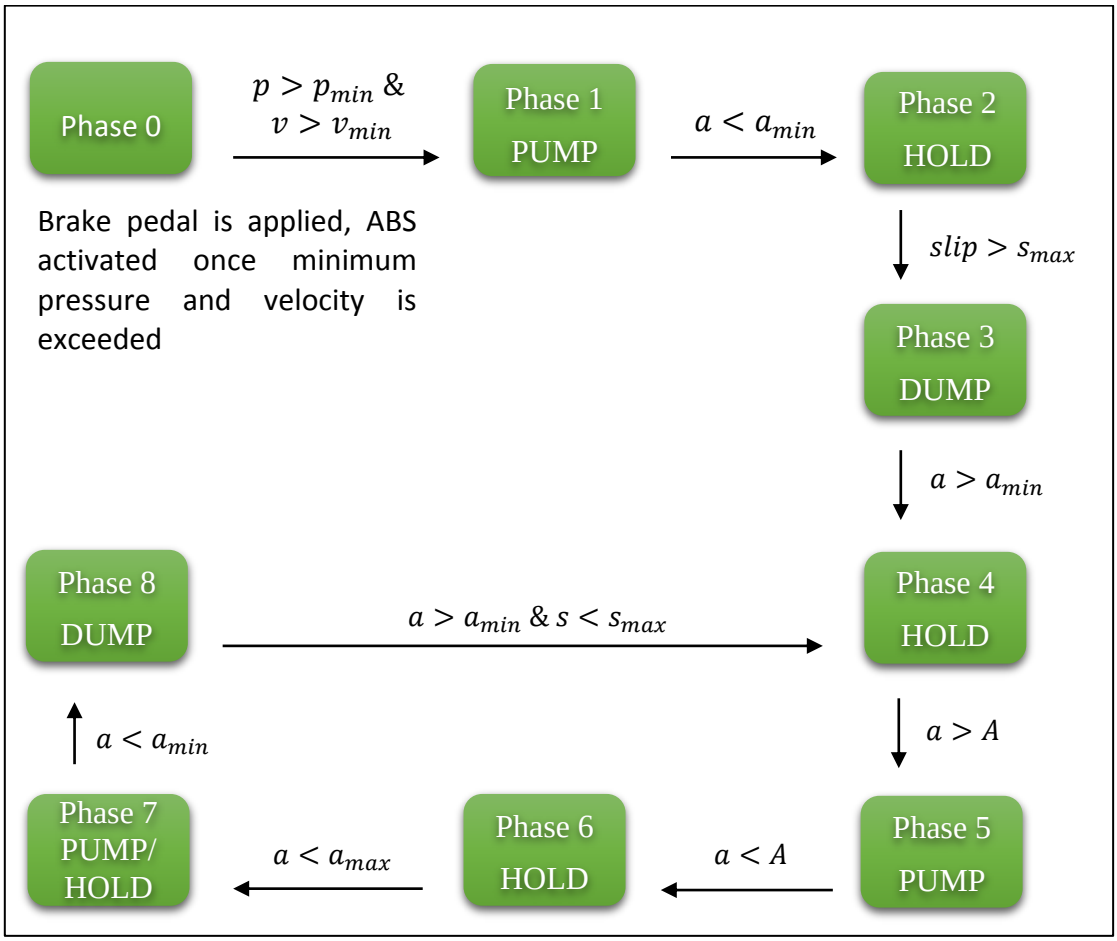

Figure 11: Bosch ABS algorithm

1.2. Modern ABS algorithms

Since the introduction of ABS into commercial vehicles, brake based stability control systems have improved immensely with varying complexity. The following control strategies highlight some of these advancements within the research of improving ABS performance.

1.2.1. ABS control using Fuzzy Logic

Fuzzy Logic is an intelligent control strategy that performs well within non-linear environments, which makes it a control strategy worth considering for ABS braking. This control strategy works on the principle of non-numeric multi-valued logic variables called linguistic variables, which aid in the control of the system's decision making. Subbulakshmi (2014) applies Fuzzy Logic to ABS control through using the wheel slip, acceleration and deceleration of the wheels as well as utilising the measurement of longitudinal deceleration of the vehicle.

1.2.2. ABS control using sliding mode controller

The sliding mode controller is known to be a robust controller. It is a non-linear control strategy that can continuously be altered through high-frequency switching control (Bhandari et al., 2012).

The controller operates based on a state-feedback control, through which control structures can be switched, based on a particular state. The wheel slip is controlled through defining the sliding surface as a function of the maximum slip and the measured slip (Bhandari et al., 2012).

A phenomenon called chattering, is potentially problematic with this sort of controller, as this causes irregular estimations that renders the controller unreliable. It was found that using a saturation function as well as taking the integral of the switching surface (Harifi et al., 2008), this phenomenon can be reduced (Bhandari et al., 2012). The desired brake torque can then be derived in terms of the sliding surface, with an added boundary layer thickness variable which is incorporated within the saturation function. This variable allows the control strategy to be adjusted manually, allowing flexibility to the system (Bhandari et al., 2012). Provided that the optimal slip is known or can be calculated, using a surface predication scheme, the sliding mode controller is able to operate competitively against other ABS control strategies such as Fuzzy-logic self-learning, Fuzzy-logic generic and neural network ABS algorithms (Bhandari et al., 2012).

1.2.3. ABS braking using hybrid control strategies

There are a variety of ABS algorithms that are being developed incorporating a hybrid of control systems. The Fuzzy sliding mode controller makes use of Fuzzy logic to reduce the chattering phenomenon inherently found with the sliding mode controller (Guo et al., 2014). The chattering phenomenon of a sliding-mode controller was also reduced through using Pulse Width Modulation (PWM) control as well as switching control (Wu and Shih, 2003).

A control strategy was also developed that utilises adaptive feedback linearization control, through using neural networks to learn the non-linearities of a braking manoeuvre (Poursamad, 2009). The stability of the controller is checked based on the Lyapunov stability theory. The controller has also been proven to perform well with transitioning terrain conditions (Poursamad, 2009).

An ABS control system has been implemented based on the wheel forces and moments through real time for rough terrain conditions (Botero et al., 2007). Numerical simulations showed a 10% reduction of vehicle stopping distance by reducing brake pressure jumps and normalizing longitudinal force variations in subsequent braking cycles.

1.2.4. Terrain identification using ABS algorithms

A study was done to identify terrain conditions using an ABS control cycle (Zheng et al., 2011), which makes use of look-up tables. The tests done were performed through applying an ABS braking procedure on two wheels, each on a different terrain, with high or low friction characteristics.

The algorithm was designed to determine which wheel is being braked on which terrain surface, by looking at how quickly each wheel takes to lock-up, as well as how the tyres respond to the pressure control of the brakes.

Surface prediction using an ABS algorithm can also be performed using the following tyre-terrain friction relation relative to the slip ratio (Burckhardt and Reimpell, 1993). This relation is a function of the vehicle speed and the slip ratio seen in equation (3).

$$\mu(\lambda) = (C_1\left(1 - e^{-C_2\lambda}\right) - c_3\lambda\ )e^{-C_4\lambda v} \quad (3)$$

Where the different coefficients (C_i) relate to the shape of the slip-friction curve (Figure 4) of a particular terrain surface as a function of slip.

A three-point method was proposed to measure the vehicle deceleration at three different slip ratios, in order to estimate the terrain surface, provided that a pre-set value was chosen for the factor C_4 (Bhandari et al., 2012). Once the terrain has been identified, the corresponding maximum slip ratio and co-efficient of friction can be selected to govern a prospective ABS algorithm.

1.3. ABS performance on rough terrains

The popularity of Sport Utility Vehicles (SUV) has increased in recent years, shifting the operation conditions of ABS onto various terrain conditions. The operation of ABS on rough terrain is a relatively new research area which is yet to be fully understood. The following literature highlight some of the factors that exist additionally when ABS is operated on rough terrain. Tyre vibrational responses during ABS operations are also investigated.

1.3.1. Terrain surface influence on wheel speed and slip estimation

Terrain roughness and the variation of friction between the tyre and the terrain surface are important factors for the analysis of ABS braking and the design of new control algorithms (Žuraulis et al., 2014).

A scientific reason as to why braking distance on rough terrains is much larger than on smooth terrains, is well defined by Hamersma and Els (2014) that state that the rough surface of the terrain causes body roll and pitch motions in the tyre which in-turn causes large fluctuations in wheel loads. This decreases the longitudinal forces on the tyres because the vertical force varies in effect, increasing the braking distance. The fluctuation of wheel speeds seemed to also vary due to terrain excitation from rough terrains and this can partially explain why ABS braking deteriorates on rough terrains (Penny and Els, 2016).

A phenomenon called the *run-in effect* is directly influenced by the severity of the fluctuation of wheel loads (Hamersma and Els, 2014). Directly after the tyre has made contact with the terrain it is relaxed and there exists a delay in the force generation process. This delay is intensified with fluctuating wheel loads.

It was found that large fluctuations in tyre vertical load, angular wheel speed and acceleration caused problems of incorrect inputs to the control logic of ABS (Marian et al., 2009).

The deterioration of ABS performance on rough terrain was analysed through using both a test vehicle and a simulation model (Penny and Els, 2016). It was found that the main factors causing the deterioration of ABS on rough terrain was the accurate measurement of vehicle speed during experimental tests and the existing response delays within the braking system during modelling.

The slip estimation also fluctuates and thus becomes very noisy. Various filtering techniques exist that aid in obtaining cleaner signals for the wheel speeds to approximate slip. Work done on ABS for electric powered vehicles (Ivanov et al., 2015) introduced a desensitization factor that proved to be important for ABS design in a continuous wheel slip control function.

In transient tyre behaviour (rolling of tyre), the slip applied at the axle differs from the slip based on the rotation of the tyre. During ABS braking, decreasing the speed of the vehicle, decreases the damping ratio of the wheel and thus increases the oscillations in the rotational speed (Pauwelussen, 2015). The author also highlights that there is a lag between the actual longitudinal slip at the tyre-terrain contact and the slip at the axle during repetitive braking. For this reason the tyre slip-ratio for contact force analysis should be captured by measuring tyre tread speed and ground speed at the contact patch (Botha and Els, 2015). Determination of the tyre slip-ratio directly by using digital image correlation techniques avoids the uncertainties caused by measuring inaccuracies of vehicle speed and tyre roll radius due to terrain roughness.

1.3.2. Tyre Vibration response

The excitation of tyre torsional modes on rough terrains has an effect on the estimation of slip (Penny and Els, 2016).

The comparison between the vibrational response of a rolling tyre with terrain excitations and a non-rolling tyre, showed that the terrain excitations mainly excite the tyre in the frequency band below $300Hz$ (Kindt et al., 2009). This research found that the excitation amplitude dependency is restricted to the tyre's sidewall stiffness.

Rolling tyre vibration measurements were performed (Tsujiuchi et al., 2004) and it was found that the vibrational velocity of the tyre's leading edge is higher than the trailing edge. The most dominant peaks of vibration based on the velocity of a rolling tyre, were found to between $70Hz$ and $150Hz$.

Experimental measurements and modelling based on cylindrical shell theory (Koizumi et al., 2010), found that tyre rotation has no effect on the first vibration mode. Further modes in range of $50-300Hz$, have been influenced by loading and rotation conditions.

Research was conducted with a SWIFT rigid ring tyre model to investigate ABS braking performance, detected tyre resonances near $30Hz$ and $75Hz$ which match the tyre's in-plane and out-of-plane rotational modes (Pauwelussen et al., 2003).

The non-linearities of the slip, tyre contact patch relaxation length and the vertical load dependency of the dynamic tyre radius, were determined using a rigid ring tyre model in a braking torque variations study (Zegelaar, 1998). The work done on the frequency response function of longitudinal forces for different brake variations, found modes of 35, 80, 90 and $100Hz$ (Zegelaar, 1998). From the frequency response of slip variation data, a first resonance frequency of $65Hz$ was determined.

The torsional dynamics of a tyre can have a negative influence on the measurement of wheel speeds and the estimation of slip. A study was done on the sensitivity of a cut-off frequency, on the measurement of wheel speed, to an ABS controller (Adcox et al., 2012) and it was found that cut-off frequencies lower than $15Hz$ removed most of the tyre-wheel dynamics and decreased the stopping distance of the vehicle.

1.3.3. Influence of tyre structure

The properties of an SUV tyre's sidewall has different influences on its vibrational characteristics. By increasing the apex length and the carcass width, the vibration energy can be decreased, whereas by increasing the sidewall gauge and the apex hardness, the vibrational energy can be decreased (Lee and Kim, 2008).

Sivaramakrishnan et al. (2015) performed an experimental study of the influence of tyre design parameters such as carcass stiffness, tread compound and tread stiffness on the performance of ABS, highlighting that the peak grip, braking stiffness, optimal slip ratio and the shape factor are the main contributing characteristics. The braking stiffness is expressed as a combination of carcass stiffness and tread stiffness, where the latter is a dominant factor during the initial braking cycles in the pressure build up phase. The first cycle of braking can cause the most loss in the stopping distance and thus the braking stiffness is a significant parameter in ABS performance. The tread compound also has a large influence on the efficiency of the ABS algorithm.

1.3.4. Suspension settings on ABS performance

Investigations have been done in improving the braking performance of ABS on rough terrain, through altering the stiffness and damping settings of a vehicle's suspension (Hamersma and Els, 2014). The suspension settings of a vehicle were changed through using a hydro-pneumatic semi-active suspension.

Numerous tests with different suspension characteristic combinations were performed and it was found that the braking distance between the worst and the best suspension configurations was $9m$, braking from $80km/h$ to $10km/h$. Further advances in this control strategy can be carried out using continuous damping along with an accommodating ABS algorithm.

1.4. Conclusion

This literature study concludes the research found on ABS braking on rough terrain. Key factors that play a role in the performance of ABS on rough terrain are fluctuations found in the vertical loads of the tyre, as well as fluctuations in wheel speed. It is thus important that adequate measuring techniques are used for the measurement of wheel speed and the measurement of tyre forces, to better understand rough terrain influences on ABS.

Based on the literature found the main aims of this study were identified. The first aim was to improve the measurement of wheel speeds which have a direct effect on the estimation of vehicle speed (if derived from wheel speeds) as well as the estimation of slip.

Two main aspects exist in quantifying the reliability of wheel speed measurement, these are the amount of noise that exists within the signal and the response time of the measurement equipment. Any noise in the wheel speed measurements are magnified when the wheel speeds are derived to calculate wheel accelerations. Driving on rough terrain can also induce further noise on the measurement of wheel speed, thus it is important that the measurement technique is robust, especially for rough terrain. Fast response time is important as sudden changes in wheel speeds during ABS exists and it is imperative that the speed is measured with the least amount of delay.

The second aim of this study is to investigate tyre-terrain interaction through looking at tyre forces during ABS braking on smooth terrain as well as on Belgian paving. It was found in literature that fluctuating wheel loads play a role in the efficiency of ABS braking, thus it is necessary to use an experimental setup that is able to isolate the tyre-terrain interaction. A validated simulation model of the experimental setup will also aid in this investigation.

The following chapters of this study will be discussed briefly. In Chapter 2, an investigation of the measurement of wheel speed, that encompasses vehicle speed and slip estimation, is performed.

A feasible solution to the measurement of wheel speed, which addresses the issues of noise and response time, is investigated. In Chapter 3, the experimental setup is conceptualised, constructed and instrumented. The mass and inertia properties of the setup are also measured.

Chapter 4 covers the work done on building a simulation model based on the measured mass properties of the experimental setup and validating the model with experimental tests. In Chapter 5, experimental and simulated ABS braking tests were performed and tyre frequency responses, during experimental ABS braking, were investigated. Chapter 6 concludes this study and a few recommendations are mentioned for further investigations.

2. Wheel speed measurement investigation

The most important parameter for ABS is wheel speed and it is thus imperative that the measurement technique used, is robust and accurate. One of the main factors that Penny struggled with when testing ABS on rough terrain, was the measurement of wheel speed (Penny and Els, 2016). The first aim of this study is to investigate how this could be improved. Wheel speed and vehicle speed measurement techniques are also discussed.

2.1.1. Method of Wheel speed measurement investigation

The standard hardware utilised to measure wheel speed in commercial vehicles, are variable reluctance sensors that generate a signal when a serrated object is rotated in close proximity to the sensor. The standard components on a Land Rover Defender make use of the variable reluctance sensors that pick up serrations, that are either a CV joint (front wheel) or a reluctance ring inside the wheel hub (rear wheel).

Figure 12: Serrated CV joints

Figure 13: Rear wheel hub with reluctor rings

The voltage signals vary as the strength and direction of the magnetic field changes, producing a variable reluctance signal, which is a signal that increases in frequency and amplitude as the triggering of the signal is increased. This signal needs to be conditioned and converted to wheel speeds.

Conventionally the signals from the wheel speed sensors are conditioned within the ECU of the vehicle. For this study, two different electrical circuits were used to condition the wheel speed signal, rather than using a commercial ECU. An additional circuits was built to convert the variable reluctance signals of the variable reluctance signal, to an output voltage relating to wheel speed. This was done using a LM1815 which is a variable reluctance amplifier. The circuit converts the variable reluctance signal to a pulse signal.

Using this amplifier, the variable amplitude of the wheel sensor signals are eliminated whilst the frequency content is still maintained. The circuit produces a one-shot pulse output signal, which corresponds to the zero crossing of a set reference voltage of the variable reluctance input (Texas Instruments Incorporated, 2013). The pulse width, τ_{pulse}, of the output is designed by the selection of a capacitor and a resistor using the following relation (Texas Instruments Incorporated, 2013).

$$\tau_{pulse} = 0.673 \times R \times C \quad (4)$$

The Land Rover defender vehicle, which is used as a case study, is assumed to travel at a maximum speed of $140km/h$. There are 60 serrations for one rotation of the wheel, generating 60 pulses. Finding the angular velocity of the wheel is done through using a wheel radius of $0.38m$.

$$\omega = v/R_{eff} = \frac{38.89m/s}{0.38} = 102.34\, rad/s \rightarrow 16.29\text{Hz}$$

This value (16.29Hz) is then multiplied by 60 for the number of pulses created per revolution and a frequency of $977.3Hz$ is obtained. A maximum of $1kHz$ is chosen for the operational limit of the circuit. A resistor of $150k\Omega$ and a capacitor of $4.7nF$ for a pulse width of $0.5ms$ ($1kHz$) was selected.

The conditioning of the pulse signal was tested using two prototype methods. The first method used a ADVFC32KNZ analogue frequency to voltage converter and the second method used a dsPIC33 which makes use of a programming a dsPIC to use its interrupt pin to convert the pulse signal. This is done through essentially timing the delay between pulses and converting the delay to a frequency and sending an output voltage scaled from 0 to $3.2V$, with a frequency range from $0Hz$ to $1kHz$. This circuit has an added advantage in tune-ability as the dsPIC33 can be programmed to adjust the output voltage, relative to a voltage range. The dsPIC33's resolution can also be altered.

Tests were performed on a front axle serrated CV joint (Figure 15), using a standard ABS sensor. The CV joint was fitted onto a CNC machine and the ABS sensor was triggered by the serrations on the CV joint. Additional sensors were added to the test setup namely, a retroreflective sensor which was triggered by a small piece of reflector tape situated on the rotating object and a proximity sensor which was triggered by an additional gear fitted to the CV joint. An IncOder sensor from Zettlex was also added to the test setup (Zettlex, 2018). These sensors operate like inductive angle encoders, which has two parts (Figure 14), a stator (stationary disc) and a rotor (rotating disc).

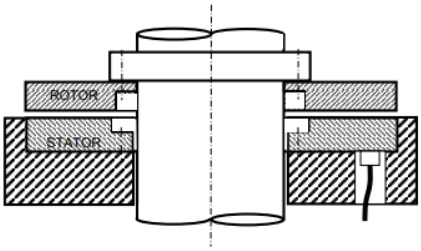

Figure 14: IncOder Zettex setup (adapted from Zettlex (2018))

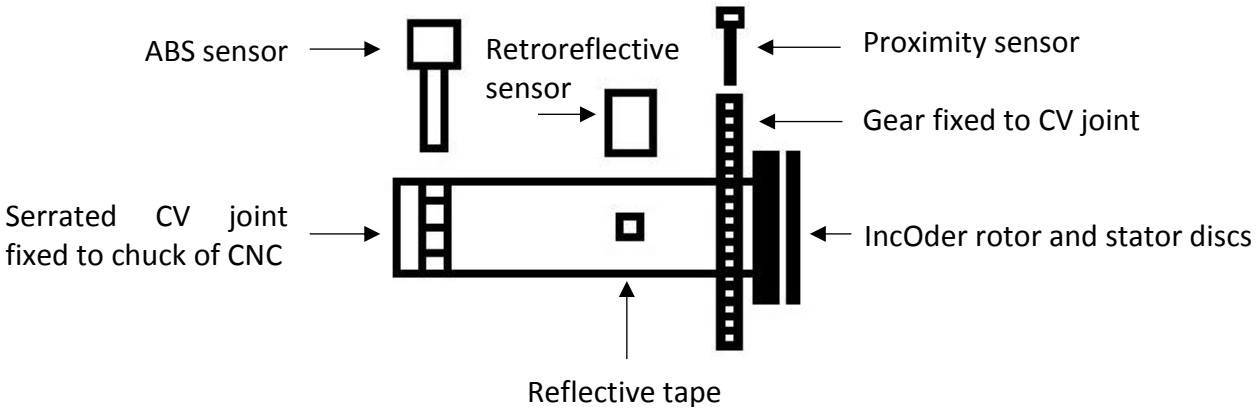

Figure 15: CV joint CNC test setup

The pulse generating circuit (LM1815) as well as the frequency to voltage circuits (dsPIC and ADVFC32KNZ chip) were used to condition the variable reluctance analogue signal from the ABS sensor. The retroreflective and proximity sensors were measured from their analogue pulse signals and through post-processing converted to angular speed. The analogue signals from the IncOder reflected the angles measured and were also post-processed to obtain the speed. Once all signals were conditioned their angular speed measurements were compared. The measurement of the signals is summarised in Figure 16.

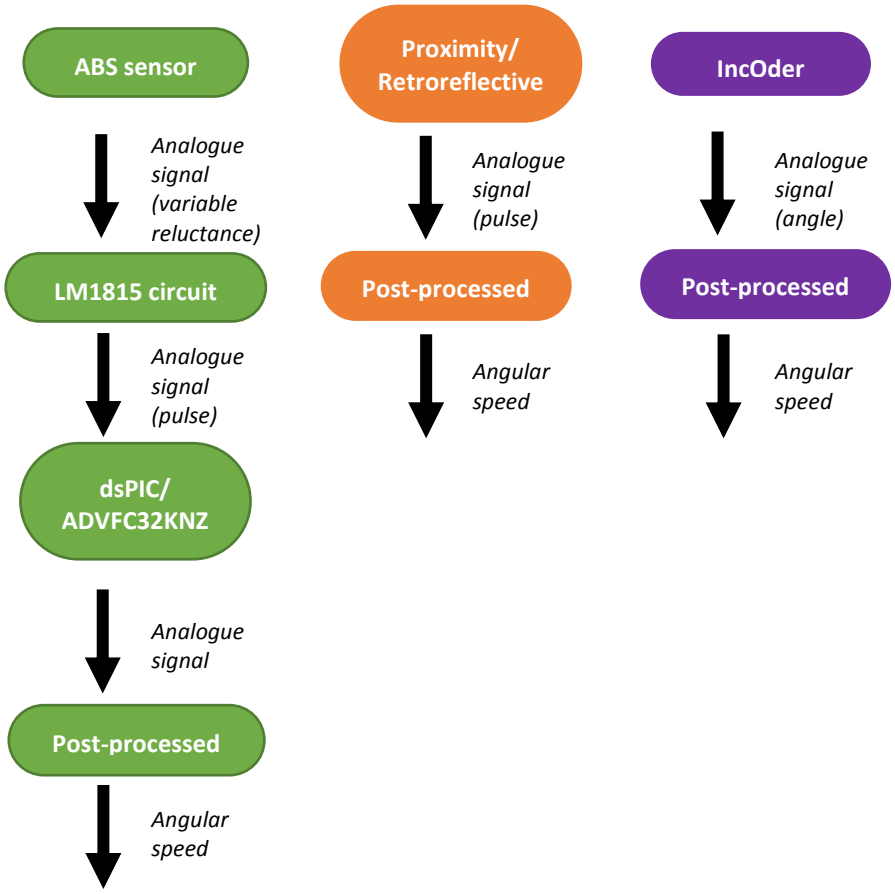

Figure 16: Signal processing of sensors

The initial test showed very noisy results, due to the LM1815 not filtering the signal effectively, allowing most of the noise to be carried through to the dsPIC signal. It was also later found that the ABS sensor was not fixed properly and would sometimes skip a pulse. The effective response times of the DSPIC and encoder were also difficult to determine as the signals were quite erratic (Figure 17).

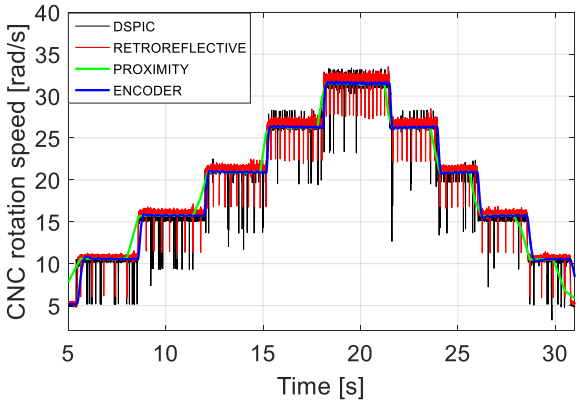

Figure 17: CNC wheel speed test

The initial challenges were addressed and it was found that the dsPIC performed much better than the ADVFC32KNZ circuit, as the DSPIC produced a much cleaner signal (Figure 18). The ABS sensor was chosen as it is the most robust sensor particularly for rough terrain.

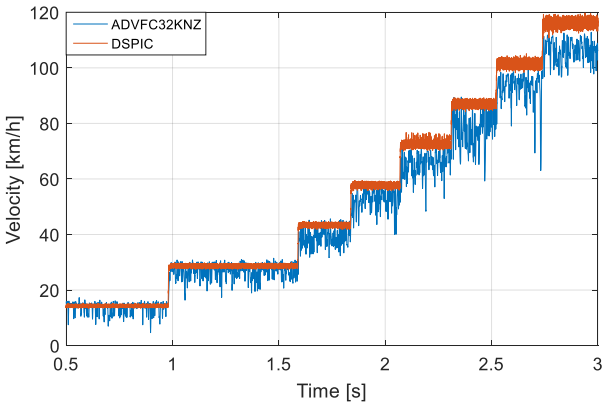

Figure 18: DSPIC readings on CNC converted to vehicle speed

The dsPIC circuit along with the variable reluctance circuit was further investigated, using a signal generator to look at the quality of the dsPIC signal. Figure 19 and Figure 20 show the response of the dsPIC at increasing intervals of $100Hz$ and $20Hz$ to inspect the response of the dsPIC to the magnitude of change in the signal.

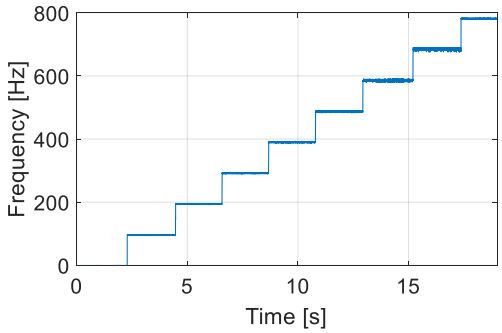

Figure 19: DSPIC signal generator test (steps of 100Hz)

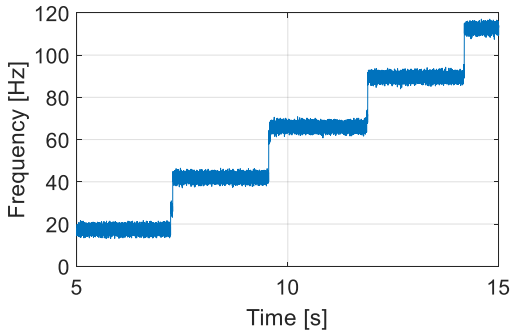

Figure 20: DSPIC signal generator test (steps of 20Hz)

The dsPIC circuit produces a clean signal with a quick response time. To derive a quantifiable value for the response time is difficult, the delay in the signal generator is not known, however in Figure 21 it is indicated that taking into account all the delays present including that of the LM1815 circuit, the response time is roughly 1ms. If the signal is converted to wheel speed in terms of km/h, then an error of 0.3 km/h is found for a constant speed (Figure 22). Hereby it can be concluded that through using dsPIC, the aim of measuring wheel speeds is achieved through a clean, quick response analogue signal.

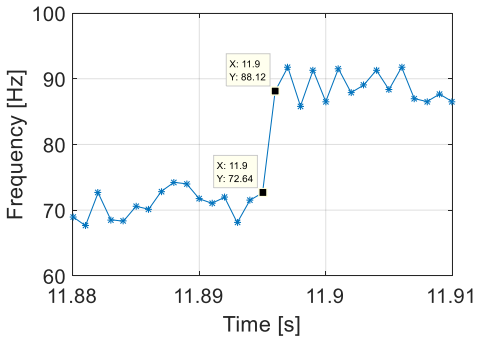

Figure 21: DSPIC signal generator tests delay with 20Hz step

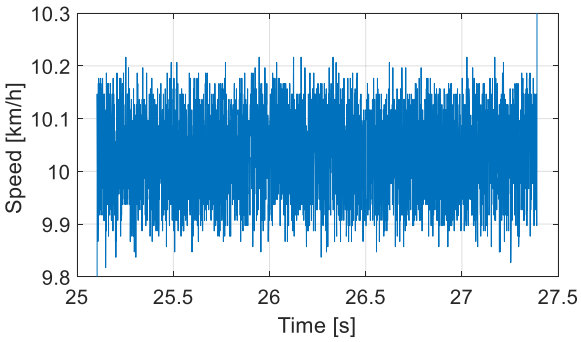

Figure 22: Wheel speed error with DSPIC

The dsPIC made some errors at estimating very low speeds (slower than $1km/h$), as the LM1815 circuit created false peaks due to noise. To solve this the dsPIC was coded to identify such occurrences, by validating the average absolute value of the raw reluctance signal and the frequency calculated from the false peaks. If the average absolute value of raw signal from the Hall effect sensors, is below a threshold of $40mV$, relating to a speed of $1.8m/s$, or if the frequency calculated is below a $3Hz$, the circuit was to bring the wheel speeds to zero. This was to avoid unwanted spikes in the speed measurements that were previously recorded at very low speeds.

Due to the fact that noise on the wheel speeds could be amplified if derived to find the accelerations, there is a need to effectively measure and filter the wheel speeds.

A digital filter used by Penny and Els (2016) and designed by Liu et al. (2004), was used to filter wheel velocities from ABS sensors. The filter basically adds a small portion of the previous recorded information to the present recorded information, creating a smoothing effect.

Careful selection of the intensity of smoothing should be considered, as the delay in the signal is increased as the signal is filtered more severely. Equation (5) shows the parameters of the filter. The symbol, y represents the unfiltered signal and yf, the filtered signal.

$$yf_i = \beta(y_i + (1-\beta))yf_{i-1} \quad (5)$$

The parameter β is selected between 0 and 1, where 0 would produce a highly filtered signal, with a large delay.

2.1.2. Vehicle speed estimation for slip calculation

The longitudinal slip is a relation between vehicle speed and wheel speed (equation (1)). The angular wheel speeds are converted to peripheral speed through the assumption of an effective rolling radius. It is possible to derive vehicle speed from the wheel speed. There are however inaccuracies that arise when the wheels start to lock-up or when they fluctuate due to the control of ABS.

The assumption for an effective rolling radius is also not always accurate especially for driving on rough terrain, where the rolling radius fluctuates.

Various vehicle speed approximation techniques exist, varying in number of input measurements and complexity. The first estimation method for vehicle speed is through using an Adaptive Nonlinear filter approach (Jiang and Gao, 2000). This principle is efficient and simple as it only requires the wheel speeds as an input. The vehicle speed is assumed to be equal to the wheel angular velocity, multiplied by the wheel's effective rolling radius when no braking is applied.

$$v_w = \omega R_{eff} \tag{6}$$

When braking occurs, slip is generated, resulting in a non-linear relationship between the vehicle speed and the wheels. The filter is said to act as a bang-bang controller that continuously updates the deceleration constant (R_d), to reflect the terrain condition and in turn the deceleration rate of the vehicle ($\dot{v}$). The deceleration constant (R_d), is estimated at the peaks of the wheel velocities as the vehicle speed is very close to the wheel velocities at these locations. The vehicle's velocity is approximated using the following non-linear filter (Jiang and Gao, 2000).

$$\dot{v}(t) = -R_d \cdot sign(v(t) - v_w(t)) \tag{7}$$

The input and output of the equation, v_w and v, relate to the wheel speed and the vehicle speed respectively. As the deceleration of the vehicle cannot be greater than μg, the approximation of the deceleration constant is restricted to a maximum deceleration of $1g$, as μ seldomly exceeds 1 under normal conditions. If the velocity of the wheels exceed the velocity of the vehicle, the velocity of the vehicle is set equal to that of the wheels.

To make the approximation of the deceleration constant less susceptible to noisy peaks, it is always taken as the slope between the starting point and the current peak.

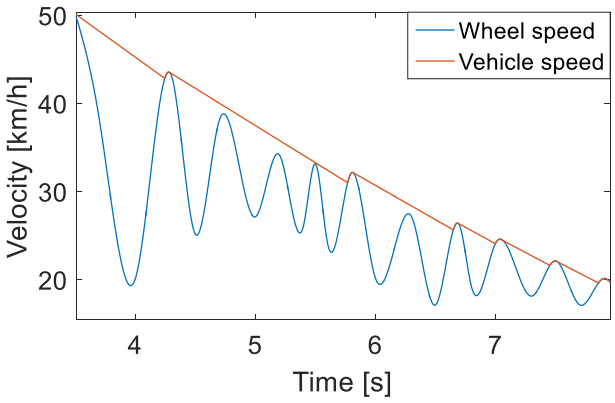

Figure 23: Example of an adaptive non-linear filter

Figure 23 is created for illustration purposes, using a fixed deceleration constant value. It is suspected that for a relatively clean wheel speed signal, the digital filter would perform as required. If a considerable amount of noise exists within the signal, however, the filter could become unstable, especially if there is a substantial presence of spikes.

Kalman filtering (Daid and Kiencke, 1995) can also be used to estimate vehicle speed. This type of filter uses additional sensors such as accelerometers, in conjunction with wheel speed sensors, to allow effective filtering of noise present in the wheel speeds.

This filter in effect averages each input with a certain weighting, relative to the most reliable sensor (Daid and Kiencke, 1995). This method of filtering the data from various sensors could prove to be beneficial, especially with braking on rough terrains, where an elevated amount of noise can be expected from wheel speed fluctuations as well as noise from accelerometers.

Using data fusion with a Kalman estimator, (Amiri and Moaveni, 2012), it was found that a high accuracy in vehicle speed estimation could be achieved, as opposed to Adaptive filters, which have errors due to distortion and are more susceptible to fluctuations. The data fusion Kalman filtering study was done using a LuGre friction model to calculate the input wheel speeds.

Fuzzy estimators are used to estimate the vehicle speed using a similar approach as the Kalman filter estimator. A Fuzzy estimator uses data fusion to estimate slip through estimating the vehicle speed, through the use of all four wheel speed sensors and an accelerometer that measures the longitudinal acceleration of the vehicle (Subbulakshmi, 2014). Data fusion is done through firstly determining which wheel sensor is delivering the most reliable information and secondly determines how reliable the accelerometer is. The weighting of the inputs are set relative to the vehicle's driving condition. In a braking condition, the wheel speed measurements are weighted low to account for the wheel deceleration and existing fluctuations, where in a constant speed driving condition, the accelerometer measurements can be set to a relative low weighting.

Further vehicle estimations were also achieved by combining Fuzzy logic with Kalman filtering. The Kalman filter is used to filter out the noise in the system and address the uncertainty of the speed and acceleration measurements. The Fuzzy logic method is used to tune the filter relative to detected slip conditions (Kobayashi et al., 1995).

A GPS tracking unit, such as a VBOX3, may also be utilised to measure vehicle speed. The VBOX3 (Racelogic limited, 2011) has a velocity accuracy of $0.1km/h$, a velocity resolution of $0.01km/h$ and a latency of $12.5ms$.

Such a device is applicable for the research in this study as it is necessary to measure vehicle speed accurately. Though using a VBOX, the assumption for an effective rolling radius does not have to be considered for vehicle speed, but only for the estimation of slip, where the angular wheel speeds have to be multiplied by the effective rolling radius.

2.2. Conclusion

Measurement techniques for ABS were investigated and the different methods of conditioning the wheel speeds, using a standard Land Rover ABS components, was performed. Additional sensors were used to compare the measurement of angular speed of the ABS sensors. Through using a LM1815 chip as well as a dsPIC the wheel speeds could be measured with an acceptable level of accuracy and response time.

The measurement of vehicle speed is to be measured using a VBOX3. This allows high accuracy and low latency and also eliminates inaccuracies that occur during ABS braking on rough terrain.

The estimation of slip is thus performed using wheel speed, measured by variable reluctance sensors, and vehicle speed, measured by GPS. The assumption of an effective rolling radius will still exist with the calculation of peripheral speed of the wheels, equation (1), when estimating slip. Through using a GPS device to measure vehicle speed however, the accuracy of the estimation of slip is increased.

3. Experimental setup

After a feasible method of measuring wheel speed and vehicle speed was found an appropriate experimental setup had to be chosen.

The second aim of this study was to investigate ABS performance on rough terrain by focussing on the tyre-terrain interface. To allow this isolated investigation, the experimental setup had to have relatively few unknowns, as it was important that all influences on experimental tests were to be understood and quantified. This research platform was also to be modelled so that it could be used in further research to develop of-road ABS control strategies.

In a full vehicle experimental setup, too many unknowns existed and are difficult to model. An ABS trailer was suggested as it encompassed realistic vehicle dynamics of a full vehicle, but is relatively simple to model. An ABS test can also be performed for a longer duration using the trailer because the speed can be maintained by the tow vehicle. The trailer was made from an actual Land Rover Defender chassis, and was installed with standard ABS braking components mirroring an actual Land Rover Defender. The trailer was loaded to the same wheel loads that the tyres on the vehicle experiences.

In order to enable simulation based research, the trailer was to be fully modelled and validated. The trailer was constructed to have two different suspension configurations. The first is a rigid suspension, which although limits the testing speed of the trailer, allows all the braking dynamics to be translated to only the tyre itself, allowing an isolated approach to investigating tyre and terrain interaction during an ABS braking maneuverer. The second suspension configuration consists of standard spring and dampers that replace the rigid suspension which could be used for high speed tests on rough terrain. Validation tests for both suspension setups were performed and through this the accuracy of the simulated model was ascertained.

3.1. Trailer mass property and inertia tests

In order to develop a multi-body dynamics simulation model of the test trailer in MSC ADAMS, measured Centre of Gravity (CG) positions and the moments of inertia were required. The centre of gravity was calculated through pivoting the trailer about the rear axle and measuring the change in the weight (Mg), measured by a scale, relative to the change in the slope (θ), as seen in Figure 24. From this the vertical and longitudinal CG across the length of the trailer could be determined. The lateral CG position was determined through measuring the weight on the two wheels, as well as on the tow hitch where the trailer is horizontally level, as it was expected to be when it is being towed.

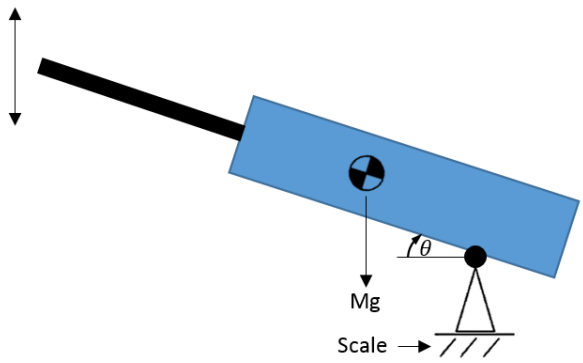

Figure 24: Determination of vertical and longitudinal centre of gravity

The moments of inertia were determined for all three axis systems (roll, pitch and yaw). The moments of inertia of the test trailer was obtained by measuring the period of oscillation about a pivoting axis (Uys et al., 2006), defined by equation (8).

$$\sum T_o = I_o \ddot{\theta} \tag{8}$$

This fundamental equation can be solved in two different methods to determine the relative inertias and both were used for improved accuracy. The first is through calculating the sum of moments by measuring the exerted force of the spring (F_{spring}) and its distance (L_{force}), from where it acts to the axis of rotation refer to equation (9) and Figure 25. The angular acceleration ($\ddot{\theta}$) also needs to be measured taking into account the distance between where the linear acceleration is measured and the pivot point (L_{accel}) shown in equation (10).

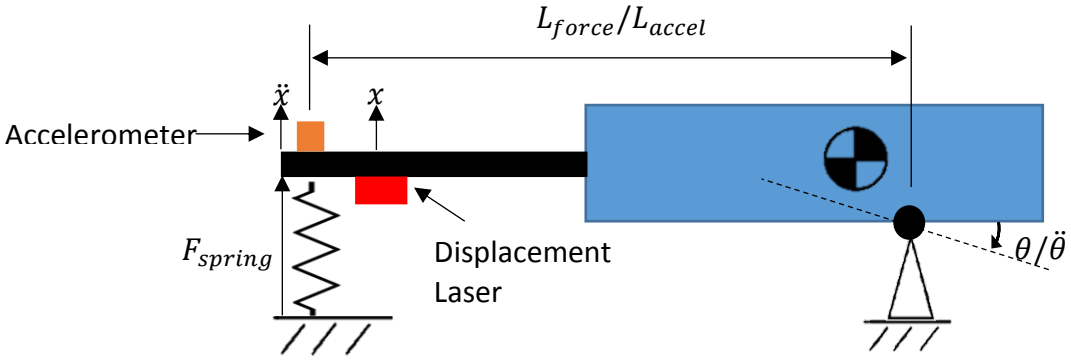

Figure 25: Moment of Inertia measurement

$$I_o = \frac{F_{spring} \times L_{force}}{\ddot{\theta}} \tag{9}$$

$$\ddot{\theta} = \frac{\ddot{x}}{L_{accel}} \tag{10}$$

The second method measures the period of oscillation and using the spring stiffness (k). The stiffness is calculated from the spring force and displacement measurements. The log decrement of the acceleration or displacement measurements (δ), calculated using equation (12), is used to calculate the damping ratio (ζ) in equation (13).

$$\sum T_o = -kL_{force}^2 \theta \ [Nm] \tag{11}$$

$$\delta = \ln\left(\frac{x_1}{x_2}\right) \tag{12}$$

$$\zeta = \frac{\delta^2}{\sqrt{\delta^2 + (2\pi)^2}} \tag{13}$$

The undamped period of oscillation (τ) is calculated with the observed damped period of oscillation (τ_d) and the damping ratio (ζ) as shown in equation (14).

$$\tau = \tau_d\sqrt{1-\zeta^2}\ [sec] \tag{14}$$

The respective inertia is calculated using the period of oscillation along with the spring stiffness and the distance between the rotating pivot axis and where the spring force is applied.

$$I_o = \frac{\tau^2 k L_{force}^2}{(2\pi)^2} \tag{15}$$

These inertias were tested through oscillating the trailer through its CG axis system, which meant that the inertias obtained did not have to be transformed as they were measured directly. Rotating about the CG axis produces large magnitudes in oscillations. If little damping exists, it also improves the accuracy of the results.

The equipment used included a load-cell attached to the trailer between the spring and the chassis, to measure the force exerted with each oscillation. A laser displacement transducer was used to measure the displacement and an accelerometer was used to measure the acceleration of each oscillation. These measurement devices were placed as close as practically possible to the where the spring was fixed.

The test results and setup can be seen in Table 3 and in Figure 26 to Figure 35 respectively. The values recorded were used to specify the geometry properties of the main body or chassis of the trailer in the MSC ADAMS model. The centre of gravity and inertias of additional parts such as the ballast weights, batteries and wheels with WFT's were measured and calculated separately and added into the model.

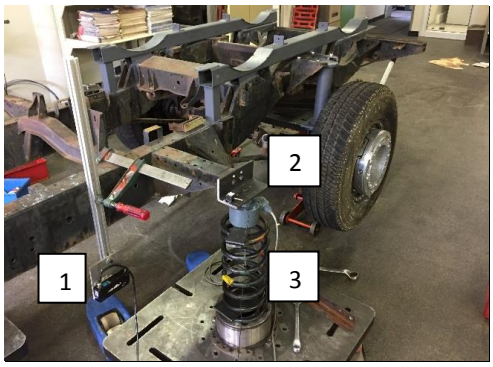

Figure 26: Determination of Roll Inertia 1 – displacement laser, 2 – accelerometer and load cell, 3 – spring

The experimental setup for the determination of roll inertia can be seen in Figure 26. The spring was attached to the side of the trailer (Figure 27), while the trailer was pivoted about the longitudinal CG axis (Figure 28).

Figure 27: Spring setup of roll inertia test

Figure 28: Pivot setup of roll inertia test

The displacement measurements (Figure 29) show that virtually no damping exists in the experimental setup. This is desired for a high level of accuracy. The spring stiffness measured is shown in Figure 30.

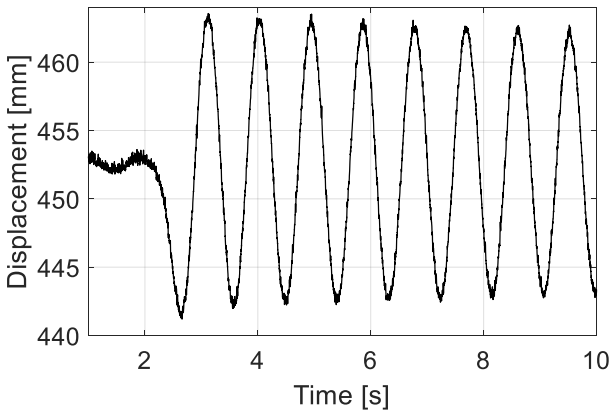

Figure 29: Roll inertia displacement

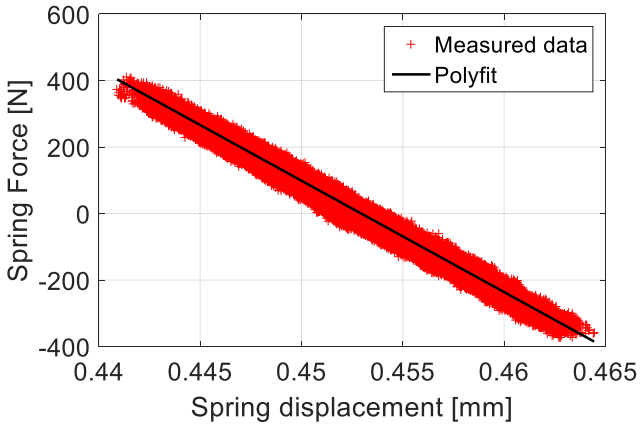

Figure 30: Roll inertia spring stiffness

To obtain the pitch inertia the trailer was pivoted about the axle positions through fixing the wheel hubs (Figure 31). The spring was fixed close to the tow hitch of the trailer (Figure 32). This was translated to the lateral CG axis, which was relatively close to this pivot position using the parallel axis theorem. The spring displacement and spring stiffness is shown in Figure 33 and Figure 34. More damping can be seen with the spring displacement as with roll, due to friction in the bearings, however the results recorded are still acceptable.

Figure 31: Pivot setup for pitch inertia

Figure 32: Spring setup of pitch inertia

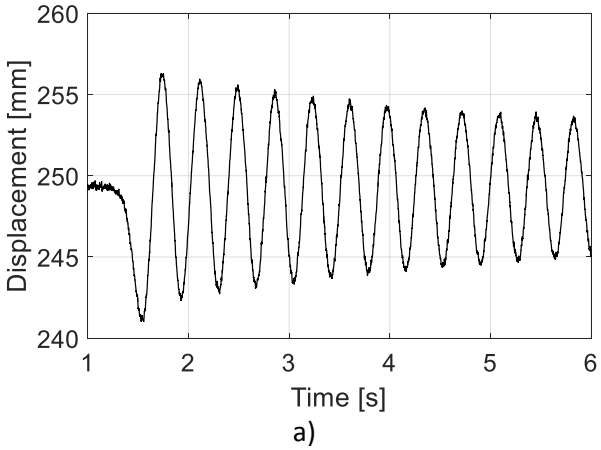

Figure 33: Pitch inertia displacement

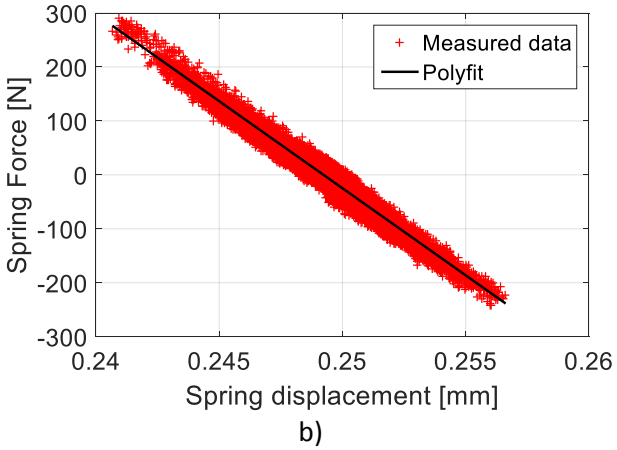

Figure 34: Pitch inertia spring stiffness

The yaw inertia was determined through attaching the tow hitch to a tow bar supported by a steel beam. The spring was attached to the rear of the trailer from the side and was supported by two bearings covered with grease to reduce the friction between the bearings and the steel platform on which they were rolled (Figure 35 and Figure 36).

Figure 35: Spring setup for yaw inertia test

Figure 36: Pivot setup for yaw inertia test

The spring displacement was quite highly damped due to the friction in the setup, however the logarithmic decrements could still be determined from the recorded data (Figure 37 and Figure 38). The accuracy of the yaw moment of inertia is also less critical for the ABS braking investigations as the trailer will rarely experience yaw motions.

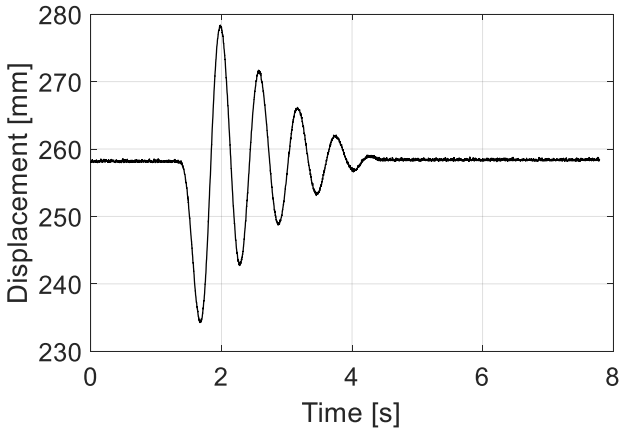

Figure 37: Pitch inertia displacement

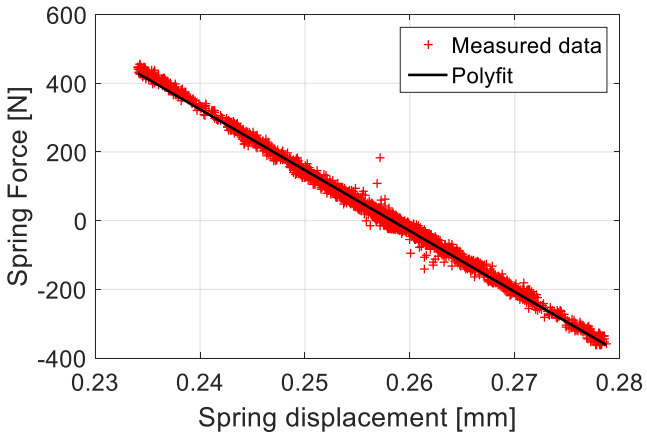

Figure 38: Pitch inertia spring stiffness

Two ballast weights were used to load the trailer and to reflect the load experienced on the tyres of a full vehicle. The mass properties and inertias of these ballast weights were also calculated. The shape of these weights were assumed to be cylindrical with uniformly distributed weight. The CG of each drum could thus be estimated to be situated directly in the centre of the drum. Each weight was weighed and their inertias were calculated using their relative dimensions and using equation (16) and (17) (Meriam and Kraige, 2007).

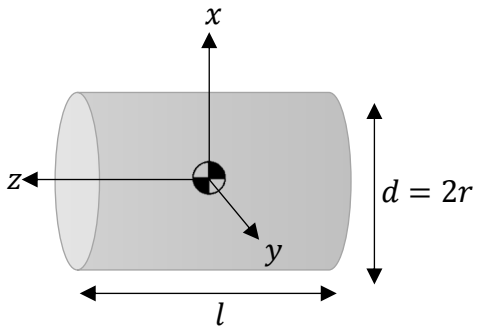

Figure 39: Ballast weight dimensions

$$I_{xx} \,/\, I_{yy} = \frac{1}{4}mr^2 + \frac{1}{12}ml^2 \tag{16}$$

$$I_{zz} = \frac{1}{2}mr^2 \tag{17}$$

Their measured mass properties and inertias are tabulated in Table 2. These calculations were compared to experimental inertia tests performed with the ballast weights attached, to check the accuracy of the experimental tests.

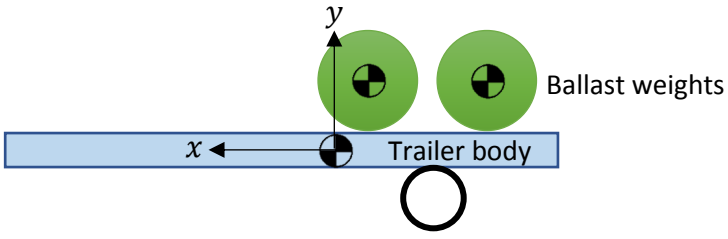

Figure 40: Schematic of Ballast weights fixed onto the trailer

Table 2: Ballast weight mass properties and inertias

Ballast weight	*Mass* (kg)	*CG of weights relative to trailer CG (using the axis system in Figure 40)*	I_{xx} / I_{yy} $(kg \cdot m4)$	I_{zz} $(kg \cdot m4)$
Weight 1	514	$-0.74, 0, 0.228$	44.7351	23.130
Weight 2	520	$-1.5, 0, 0.288$	45.2573	23.400

Four consecutive tests were done for each mode of inertia and averaged. Table 3 shows the data processed from the CG and inertia tests.

Table 3: Moments of inertia and centre of gravity of test trailer

Trailer load conditions	*Mass, kg*	*Moments of inertia, kg·m⁴ (without wheels and WFT's)*			*Centre of gravity, m*		
		I_{roll}	I_{pitch}	I_{yaw}	Longitudinal distance from the wheel axle	Lateral distance from the symmetry axis	Vertical distance from the ground
Chassis	570	66.36	887.20	3204.45	0.823	0.01	0.615
with weight 1	1027	295.21	996.65	4701.88	0.644	0.063	0.894
with weight 2	1547	476.95	1610.02	12851.40	0.223	0.042	0.986

3.2. Suspension characterisation

The trailer was fitted with standard Land Rover Defender suspension components, after it was tested and validated with rigid suspension. Before the suspension was installed onto the trailer the spring and damper components were characterised so that an appropriate suspension model could be implemented with the MSC ADAMS model.

The spring and dampers were fixed onto a hydraulic testing rig and tested relative to a displacement and velocity range to find the spring stiffness and damping characteristics. The setup is indicated in Figure 41 and Figure 42. The results for the spring and damper characterisation can be seen in Figure 43 and Figure 44.

Figure 41: Damper characterisation

Figure 42: Spring characterisation

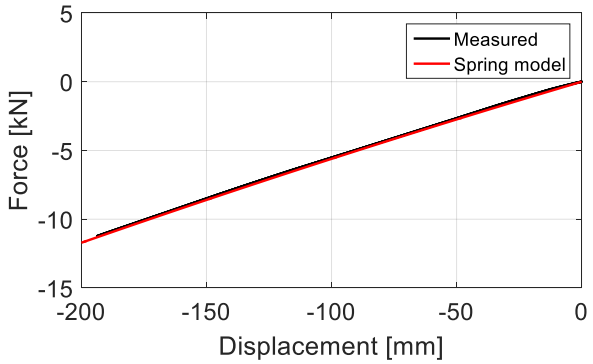

Figure 43: Spring tests compared to spring model

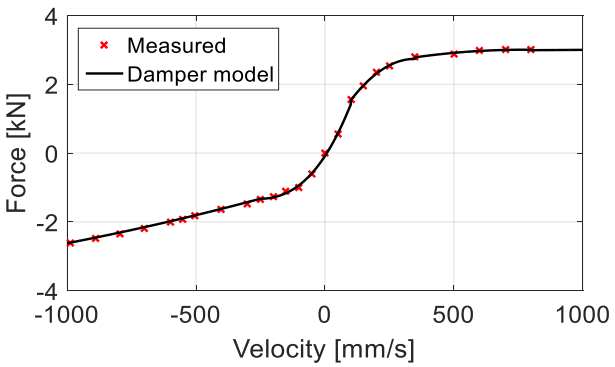

Figure 44: Damper model compared to measured data

As the damper characteristics are non-linear, the damper was modelled into MSC ADAMS through co-simulation with Simulink, using a piece-wise polynomial model. MSC ADAMS only utilises a cubic spline approximation for the measured data and this proved to be inaccurate, especially at high velocity ranges. The springs and dampers were then installed on to the testing trailer as indicated in Figure 45.

a) b)

Figure 45 a) and b): Spring and dampers installed on trailer

3.3. Instrumentation on the trailer

Instrumentation equipment which was used to measure a variety of aspects on the trailer was installed. The recording and control of each equipment used, is discussed.

3.3.1. Wheel speed and longitudinal slip measurement

Wheel speeds were measured using the standard ABS components from Land Rover, and their signals were conditioned with the circuits developed in Chapter 2. The wheel accelerations were calculated from these signals using an averaging differentiator (equation (18)). As any noise on the wheel speeds is magnified when acceleration is derived, a form of filtering the noise is necessary. This is accomplished through averaging the acceleration over a certain amount of previous values. Through this, the acceleration calculated is a lot smoother than directly differentiating the wheel speeds. A step size of 20 previous values was used, thus the acceleration was averaged over a time step of 20ms.

$$\alpha = \frac{\omega_i - \omega_{i-20}}{t_i - t_{i-20}} \tag{18}$$

With the vehicle speed being measured using a VBOX3, the longitudinal slip on the trailer's wheels was calculated through assuming a constant effective rolling radius ($0.38m$) with the measured wheel speeds.

3.3.2. Braking components

Stock standard Land Rover parts have been installed, these include an ABS modulator (without an ECU), standard front brake callipers and brake lines as well as a brake pedal-booster assembly. The pedal booster was connected to the vacuum pump supply of the towing vehicle. Additionally $25MPa$ pressure transducers were installed near the brake callipers on each brake line.

The ABS modulator that is used in a Land Rover Defender is a WABCO Modulator that includes a pump. The modulator has 15 pins that relate to a specific function. These included the control of 8 solenoids which control the pressure for the brakes. Each wheel has two valves, an inlet valve and an outlet valve. The outlet valve is a normally closed valve, which means that if no electrical power is supplied ($0V$), the valve is closed and if it is supplied with $12V$, the valve will open. The inlet valve works in the opposite manner. It is a normally open valve, which means that if the solenoid is powered with $12V$, it will close. The inlet valve allows brake fluid to flow from the inlet of the modulator to a specific brake line, whereas the outlet valve controls the flow of brake fluid between the brake line and the modulator. Each brake state is controlled through switching each valve to a certain configuration (Table 4).

Table 4: Brake state control

Brake mode	*Outlet valve voltage [V]*	*Inlet valve voltage [V]*
Pump	0	0
Dump	12	12
Hold	0	12

In *pump* mode the fluid flows from the master cylinder, through the inlet valve, which is normally-open, and is blocked by the outlet valve, which is normally-closed. This increases the brake pressure and prohibits fluid from flowing back to the modulator.

The *dump* phase closes off the inlet valve and opens the outlet valve to decrease all the pressure at the brakes.

The *hold* phase keeps both valves closed prohibiting the flow of brake fluid.

The modulator has a shuttle valve which switches each time a certain amount of pressure is exceeded in the modulator. ABS control is switched on as soon as the shuttle valve is triggered. The modulator has a pump input, which is switched on, with a supply of $12V$. The pump is usually switched on during a *pump* phase, as the modulator isolates pressure from the brake pedal.

The ABS modulator was controlled using an interface box that enables the switching of each valve through digital output pins, that relate to each solenoid valve and the pump inside the modulator, to a digital input pin connected to the MABX Ⅱ (MicroAutoBox Ⅱ). Opto-couplers and MOSFETS were used for the interfacing and switching of the $0V/5V$ digital outputs of the dSPACE, to the $0V/12V$ digital outputs (with high current demand) to the modulator. The pump was switched on using a relay.

3.3.3. Tyre force measurement

Two wheel force transducers (WFT), designed and built by the VDG at the University of Pretoria, were used on the trailer (Becker and Els, 2012). These can measure all three forces and moments experienced by the tyre. The WFT's are equipped with encoders that measure the wheel angle of rotation.

Two drums were filled with cement to make up 1 ton, to simulate the appropriate vertical load that the rear tyres experience on a Land Rover Defender. The fully loaded and equipped test trailer is shown in Figure 46. The trailer can be set up to have three different load cases. The first case is where no extra weight is added to the trailer, effectively the only weight is from the chassis itself. For the other two cases, two drums filled with concrete weighing $500kg$ each can be added individually.

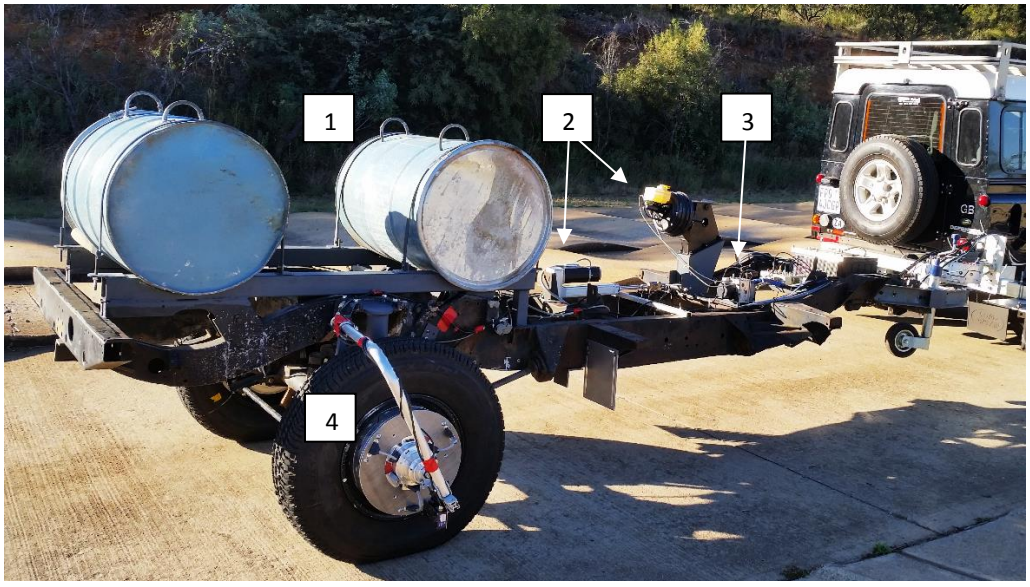

Figure 46: Test trailer fully loaded and equipped: 1 – optional loads, 2 – brake pedal with actuator, 3 – ABS modulator, 4 – wheel force transducer (WFT)

3.3.4. Control instrumentation

The ABS control and data acquisitioning is done through using a MABX Ⅱ via the Control Desk dSPACE software. This software is capable of performing various tasks such as ECU measurement, Hardware-in-the-loop and Rapid control prototyping (dSPACE, 2016).

The real time interface (RTI), which allows the automatic implementation of Simulink and Stateflow models on to the hardware, is utilised to carry out real time experiments with simulation based software. The MABX Ⅱ is equipped with an I/O port of various applications such as, analogue I/O, digital I/O, Serial Port communication and CAN bus communication.

All signals are recorded through analogue inputs to the MABX Ⅱ, except for the measurement data from the VBOX which is sent through CAN bus. The measurement of tyre forces by the WFT's are triggered by the MABX Ⅱ, but recorded independently by Helios computers within each WFT.

The brake pedal was controlled using an actuator consisting of a controllable motor and a CASM electric cylinder (linear gearbox) from Dunkermotoren (Dunkermotoren GmbH, 2015). The speed and direction of the motor was controlled with the MABX Ⅱ.

For each brake test the pedal was pulled in at the same rate and kept at the same position. Figure 47 shows the Dunkermotoren connected to the brake pedal.

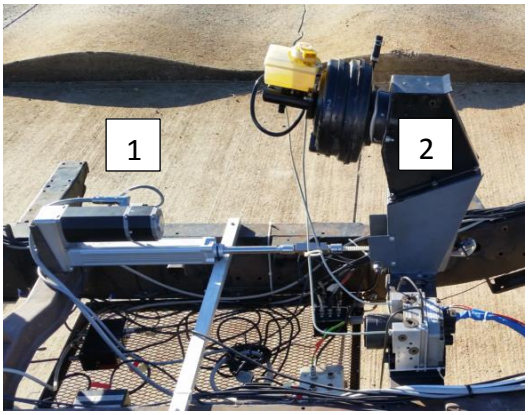

Figure 47: Pedal robot setup
1) Dunkermotoren motor and linear gearbox
2) Brake pedal and booster

The variables measured and controlled by the MABX Ⅱ are summarised in Figure 48, the instrumentation used for the measurement or control of these variables are shown in brackets. The type of signals are shown with arrows.

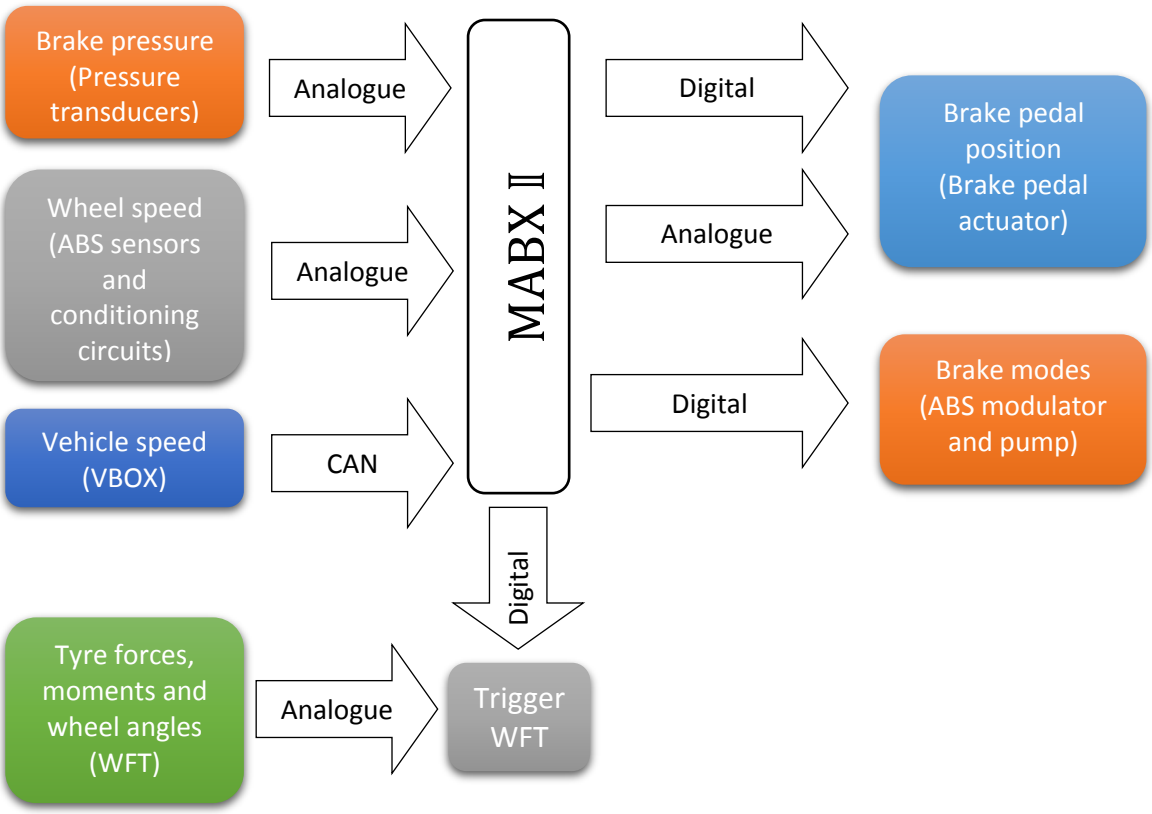

Figure 48: MABX II inputs and outputs

3.4. Conclusion

An experimental setup was conceptualised and constructed. The trailer was equipped with brake hardware in order to perform ABS braking tests and measuring equipment was installed to measure the appropriate variables during ABS braking. The mass properties and inertia of the trailer was measured and thus all parameters required to develop a multi-body dynamics of the trailer were determined.

4. MSC ADAMS model construction and validation

The model of the trailer was constructed using MSC ADAMS in co-simulation with Matlab Simulink. The Bosch algorithm, as well as the suspension forces experienced by the trailer was written and controlled in Simulink.

4.1. ADAMS model construction

The construction of the MSC ADAMS model was started once the trailer's inertias and CG positions were determined and the trailer was instrumented. The following sections describe in turn the different components of the model.

4.1.1. Trailer body

The trailer body was created with the measured inertia and CG positions, and the locations of the attachment points to the suspension and tow hitch were created (Figure 49). The ballast weights were added with their respective mass, inertias and CG positions relative to their locations on the trailer.

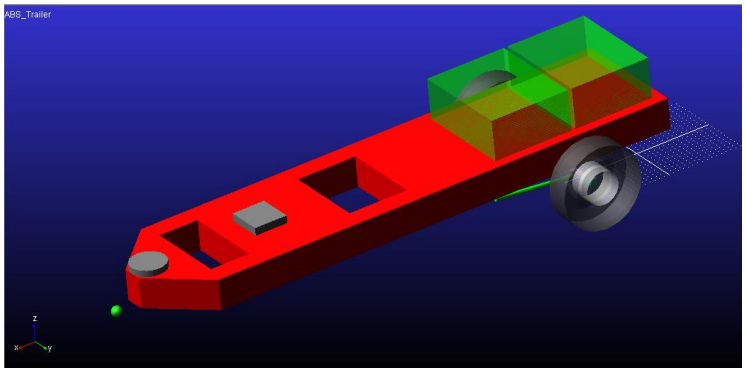

Figure 49: MSC ADAMS model of tyre test trailer with added optional loads

4.1.2. Suspension components

For the rigid suspension configuration, the axle was attached to the trailer using fixed joints at the height of the rigid suspension struts. A Land Rover Defender front axle's mass, CG and inertias were previously measured by the VDG (Uys et al., 2006).

The spring-damper suspension configuration required a trailing arm setup on the model. The attachment points for the A-arm and the two trailing arms that connect the axle to the trailer body were measured and added. The A-arm was connected to the axle with a spherical joint and a revolute joint was used to attach it to the main body (Figure 50).

The trailing arms were fixed to the axle with spherical joints and connected to the main body with torque vectors, which simulate the buffer rubbers with which the arms are held in place. These rubbers' properties were also previously measured in respect to their output torque, relative to the angle of rotation about their attachment points by the VDG (Uys et al., 2006).

The springs and dampers were implemented into the model by inserting a force between the attachment points of the axle and the body. This force was implemented through co-simulation with Simulink, by firstly reading in the displacements and velocities between the attachment points from MSC ADAMS into Simulink and then calculating the spring force, which would then be sent out to the MSC ADMAS model.

Using the suspension models with Simulink provided a more accurate method for modelling the suspension forces, as only a Cubic Spline approximation in MSC ADAMS was available for the approximation of the suspension forces.

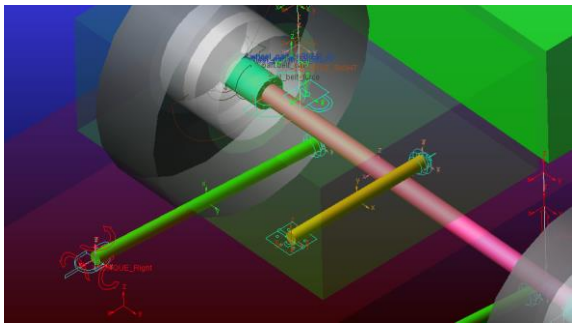

Figure 50: Trailer suspension

4.1.3. Tire model

A FTire model of the Michelin LTX A/T^2 235/85R16 SUV tyre, was incorporated into the model. This tyre model was selected because of its specific application for rough terrain conditions (Bosch et al., 2016) as well as the fact that a validated FTire model was avaliable. Parameterization data for footprint, hardness, vertical stiffness on different cleats, lateral, longitudinal and torsional stiffness and modal analysis was used to construct FTire model.

4.1.4. Terrain property files

The MSC ADAMS simulations will be performed using a class B terrain property file for the smooth terrain tests and a Belgian paving property file or off-road braking simulations. The Belgian paving can be classified as an ISO 8608 Class D terrain (International Organization for Standardization, 1995), has been fully profiled by the VDG using a mechanical profilometer (Becker and Els, 2014).

4.1.5. Pressure to torque conversion

The ABS hydraulics were simulated by converting hydraulic pressure to applied brake torque using empirical results. The pressure to torque conversion used for the MSC ADAMS model was done through measuring the braking torque during a brake test, using the WFT's and the pressure transducers.

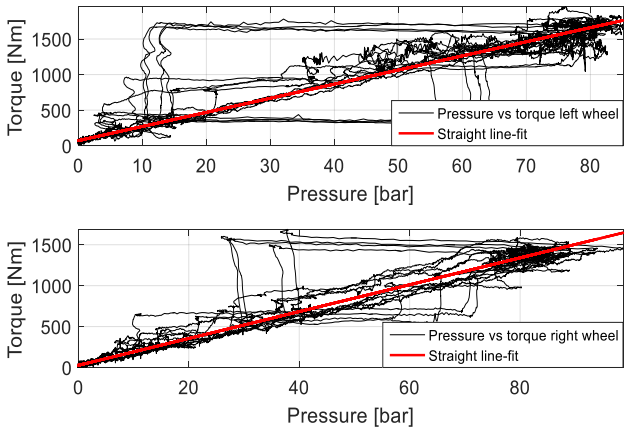

Figure 51: Pressure to torque conversion

The transfer function used in this model, prescribing the delay in pressure build-up, was measured by the VDG and used in a fully validated MSC ADAMS model of a Land Rover Defender (Hamersma and Els, 2014).

4.1.6. Degrees of freedom of the trailer

The final trailer model has 10 degrees of motion in total. These are summarized in Table 5 in terms of the main components of the model. A more detailed illustration of each body and its relative connecting joint is shown in Figure 52. The numbers next to each body and joint indicate the DOF's (for bodies) and the number of constraints (for joints).

Table 5: Trailer model degrees of freedom

Bodies	*Degrees of freedom*	*Types of motion*
Axle	2	Roll, Vertical
Chassis body	6	Roll, Pitch, yaw Lateral, Vertical, Longitudinal
Wheels	2	Rotation

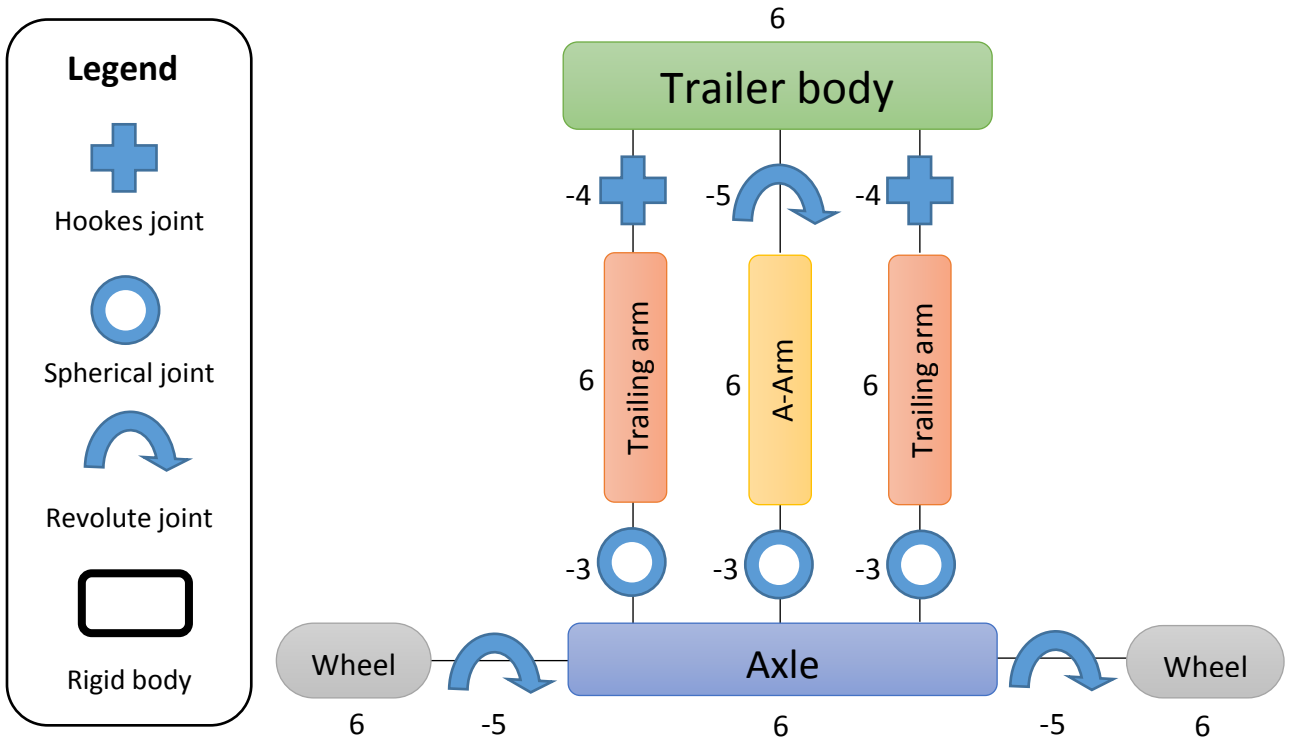

Figure 52: Graphical topology of ADAMS model's bodies and connections

4.1.7. Simulink co-simulation

The trailer model (Figure 49), was controlled through co-simulation with MATLAB Simulink and MSC ADAMS. Longitudinal, lateral and vertical positions of trailer's tow hitch and brake torques for each wheel were assigned as input values sent from Simulink. The same Bosch ABS algorithm used during experiments was to be used for brake pressure control in MSC ADAMS simulations.

4.2. MSC ADAMS model validation tests

The trailer was instrumented firstly with the rigid suspension, validated and then secondly a standard suspension setup was implemented and the trailer was again validated.

4.2.1. Trailer model validation with rigid suspension

The longitudinal and vertical forces acting on the wheel hub were identified as the most important characteristics for model validation. Model validation tests were conducted using two 100 mm high ramps to investigate tyre force response, by comparing test data with simulation data. The preliminary tests were done with no load on the trailer. By attaching the trailer to an extended beam, on the towing vehicle a lateral offset was obtained, so that only the trailer travels over the ramps, while the towing vehicle negotiated level terrain. The validation tests involving the ramps were done through driving the trailer over both ramps, that were in-line with each other, at speeds of 10km/h and 20km/h (Figure 53 and Figure 54). At 10 km/h the tyres remained in contact with the terrain but, due to the fact that the trailer has no suspension, it becomes airborne at 20 km/h as indicated in Figure 54.

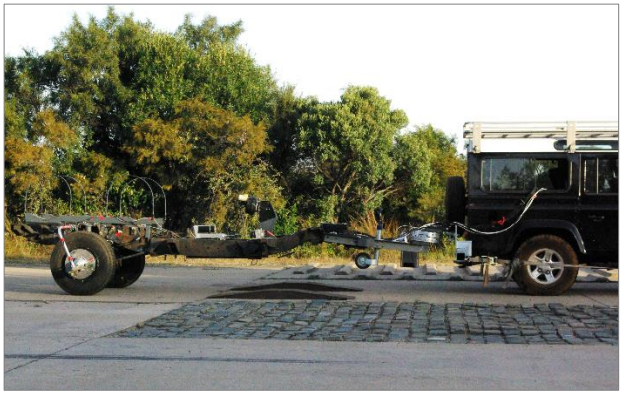

Figure 53: Model validation at $10km/h$ for rigid suspension

Figure 54: Model validation at $20km/h$ for rigid suspension

The model validation tests at $10\ km/h$ and $20\ km/h$ (Figure 55 and Figure 56), shows that the same natural frequency is excited in the two measurements and the measured tyre response of dynamic vertical force, correlates relatively well with the simulated tyre response. This shows that the inertias for the trailer has been measured and modelled correctly. The magnitude of the peaks for the measured data after the initial peak after 14.4 seconds in Figure 55, are greater than the simulated data possibly because of added dynamics from the towing vehicle.

The ramps are $1.7m$ long, thus when traveling at $20km/h$, it takes 0.3 seconds to drive over the ramp. The model validation test at $20km/h$ (Figure 56), shows that the first peak with a force of $7kN$ occurs as the trailer enters the ramp.

The measured and simulated data from the first peak up to the second (interval between 11.2 and 12.2 seconds), shows good correlation. It is within this timeframe that the trailer drives over the ramp, thus validation in terms of the trailer's interaction with the ramps is good in Figure 56. The test data shows that the response of the trailer through the excitation forces on the tyres are modelled correctly.

Figure 56 shows that, from 11.8 to 12.1 seconds, both in the simulated model and the experimental trailer, the tyre loses contact with the ramp, having zero contact force.

The experimental response of the trailer after the first peak seems too high, as usually the vehicle dynamic loads are within a range of 3-5 times static load. This could be due to the response from the towing vehicle, which is pulling the trailer with an offset, causing additional unwanted moments around the towing point. This extra excitation is speculated to bring a mismatch of the measured data with the simulated data after 12.5 seconds. This is an extreme load case.

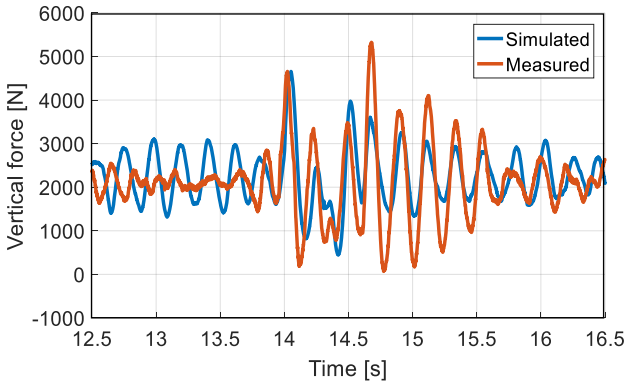

Figure 55: Vertical force using both ramps at 10 km/h for rigid suspension

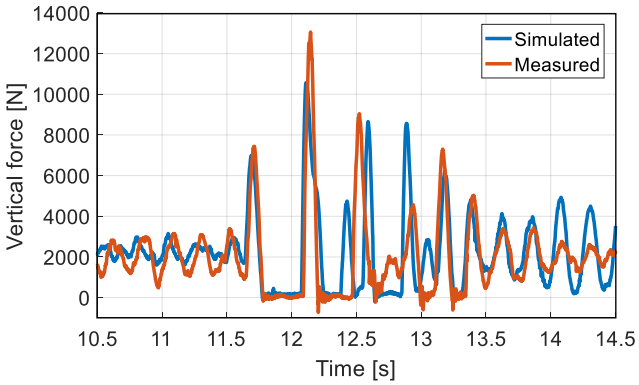

Figure 56: Vertical force using both ramps at 20 km/h for rigid suspension

The next set of data in Figure 57 and Figure 58 show braking validation tests, where the wheels were locked (ABS deactivated). The braking pressure was increased to 60 bar and kept constant for 1.5 seconds. The same measured pressure was used as input to the MSC ADAMS model. The measured braking torque as compared to the simulation model, shows the same characteristic peaks. The magnitude of the peaks are different, possibly because of a slight difference in the loading conditions for braking.

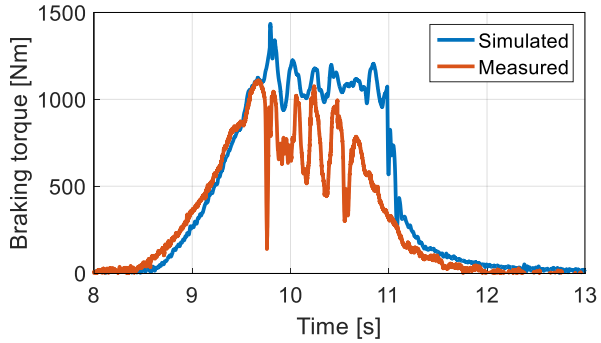

Figure 57: Braking torque for rigid suspension

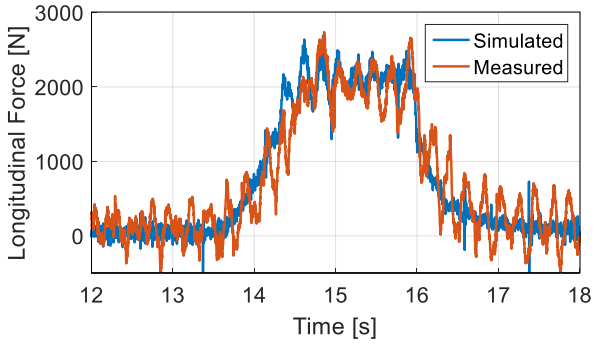

Figure 58: Longitudinal force for rigid suspension

The force characteristics show that the measured data is closely correlated with the simulated data, according to the shape of the brake force characteristic and peaks in the braking stage (Figure 58).

There are additional vibrational characteristics with the measured longitudinal force, which will be investigated in future ABS braked tyre and terrain interaction analysis.

4.2.2. Trailer model validation tests with suspension

The model validation for the installed suspension was done at a speed of 10 km/h. The results show close correlation, however for the right tyre, the measured data seems to have a higher load than the simulated data. This could be due to some inaccuracy incorporated with installing the suspension, causing the trailer to tilt slightly to the right hand side.

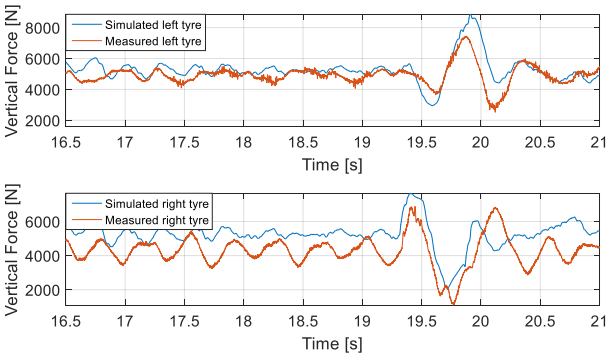

Figure 59: Model validation on ramp on right tyre

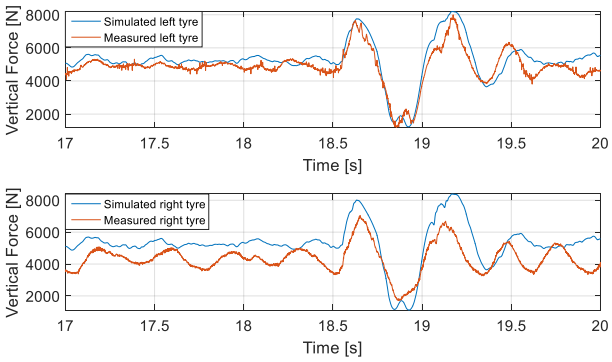

Figure 60: Model validation with both ramps

4.3. Conclusion

The validation for both suspension setups was done and adequate correlations were observed between the experimental and the simulated results. These tests show that the tyre model used was acceptable and that the trailer has been validated successfully for both vertical and longitudinal forces. ABS tests using the trailer are to be performed, where correlation between experimental tests and simulated ABS tests are to be investigated.

5. ABS braking test results

ABS tests were done on both smooth flat terrain and Belgian paving. Only one weight was used for both tests, as there was an uncertainty if enough pressure could be generated to lock the wheels on smooth terrain, to test the performance of ABS. The effect of ABS threshold values on braking performance fell out of the scope of work for this study however, a fixed value for each threshold was chosen based on literature and used for all tests and simulations. The values for the ABS thresholds used are shown in Table 6.

Table 6: ABS test parameter thresholds

Parameter	*Value*
A	$20m/s^2$
a_{max}	$5m/s^2$
a_{min}	$-50m/s^2$
s_{max}	0.2

Validation of the ABS tests were done in ADAMS, using the same pressures to inspect and compare the tyre responses of the simulation model.

5.1. Smooth terrain ABS test

The test data shown for an ABS test on smooth terrain was performed at 30km/h. In Figure 61 the wheel speeds are shown, with the vehicle speed, as well as the brake phases for the particular wheel. The wheel speeds that were measured followed the VBOX vehicle speed relatively closely when no brakes were applied. When the brakes were applied however, the wheel speeds proved to be unreliable. The measured wheel speed signals jumped up and down when the brake phases were changed from pump to dump and visa versa, particularly between the 8th and 4th phases (DUMP→HOLD) and the 6th and 7th phases (HOLD→PUMP). The oscillations in wheel speeds measured during ABS could have been caused due to the sudden changes in brake pressure.

The derived wheel accelerations and wheel slip have been extensively influenced by the phenomenon found in the wheel speeds (Figure 62 and Figure 63). The accelerations are relatively smaller in magnitude than what one can expect to see from a wheel that is controlled by ABS, as the wheel acceleration thresholds never go below the a_{min} parameter, which is governed by the 2nd, 3rd and 8th phase. This caused the algorithm to periodically get 'stuck' in the 8th phase as the a_{min} threshold was never exceeded and the wheel slip never decreased lower than the s_{max} threshold. Such an occurrence can be observed just after 32 seconds in Figure 62 and in Figure 63.

The brake pressures of this test can be observed in Figure 64. It seems that the brake system unable to effectively dump the pressure, causing the algorithm to remain in the dump phase, as neither the acceleration nor the slip remained greater than the desired thresholds, because the brake pressure was not decreased. It appears that after 3 consecutive ABS cycles, the modulator failed to cycle the pressure effectively. This occurrence coincides to where the brake phase of the left wheel gets 'stuck'.

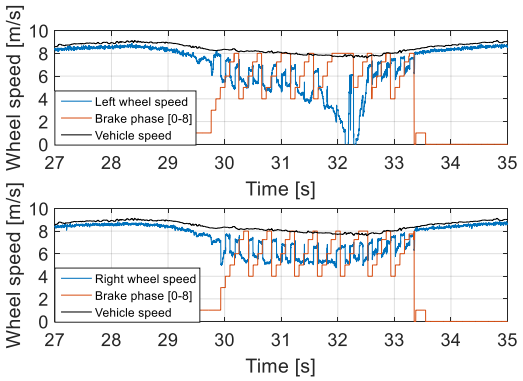

Figure 61: Wheel speeds on Smooth terrain

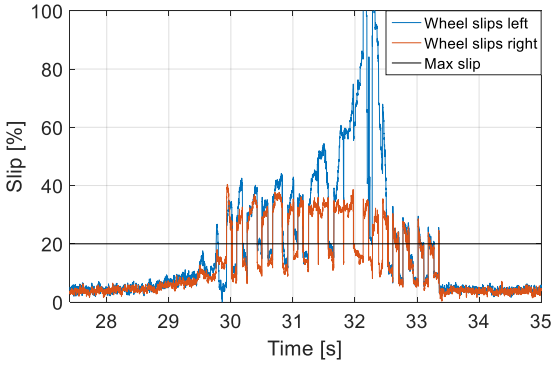

Figure 62: Wheel slips on smooth terrain

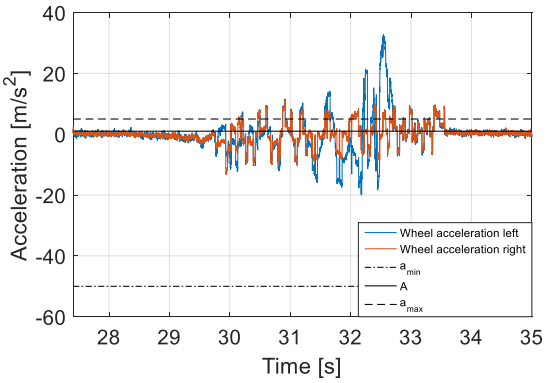

Figure 63: Wheel acceleration on smooth terrain

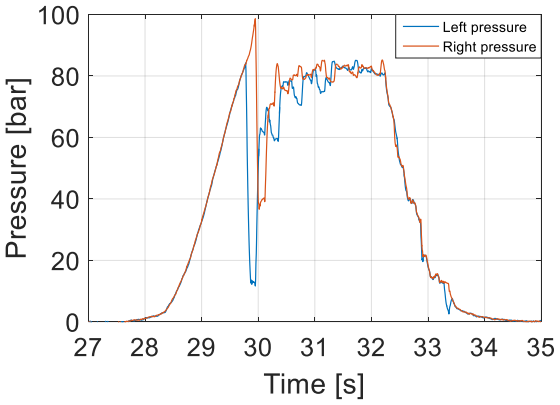

Figure 64: Brake pressures on smooth terrain

Figure 65 shows a comparison between the wheel speeds measured and the wheel speeds derived, from the encoder measurements of the WFT's. The encoders measured a similar trend to the wheel speeds, without the jumps found with the wheel speed signals. The left encoder data does show some variation of wheel speed before the left wheel locks, between 30 and 32 seconds. This comparison supports the claim that the wheel speeds do oscillate during ABS braking, to such an extent that it causes the ABS speed sensor to measure inaccurately.

Figure 66 shows the measured vertical and braking tyre forces. The initial drop in brake pressure, as ABS activates the modulator to dump the pressure, is directly reflected with the decrease in brake force at 30 seconds. It can be seen that at this instance the vertical force of the tyres increase. It can also be noted that the braking force for the left wheel, after 30 seconds, remains at a larger negative magnitude than the right wheel. This is because, from the wheel speeds measured, it could be observed that the left tyre was braked harder than the right tyre, causing the tyre to lock-up.

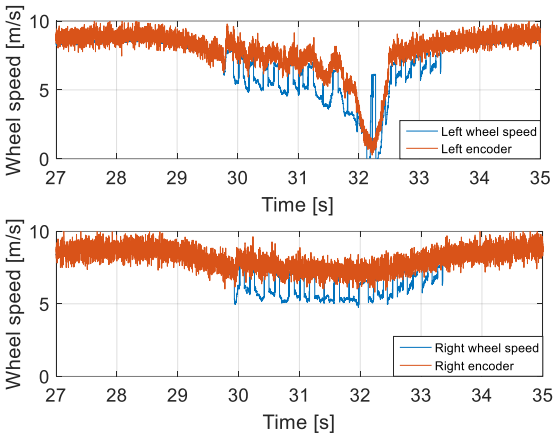

Figure 65: Wheel speeds versus encoder measurements a smooth terrain

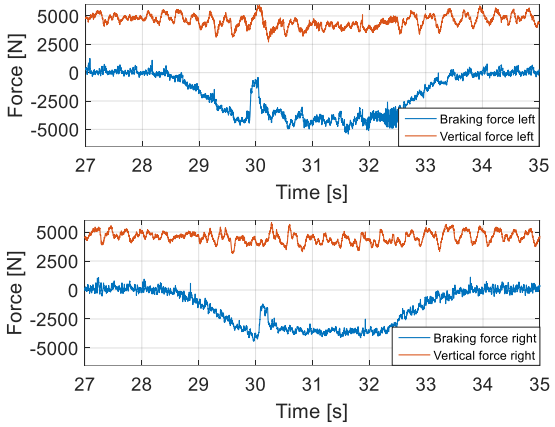

Figure 66: Tyre forces on smooth terrain

5.2. Validation of smooth terrain ABS simulation results

The simulated ABS test was completed using the measured vehicle speed and brake pressures of the experimental test as input variables to validate the ADAMS model. The trailer was driven along a terrain profile with the same class of terrain that was used as a flat terrain for the experimental test.

The measured wheel speeds are compared with the simulation wheel speeds of the FTire model in Figure 67. The simulated wheel speeds oscillate as the pressure is initially dumped at 30 seconds. These oscillations substantiate the claim that the high oscillations cause the jumps in the measurement of wheel speed.

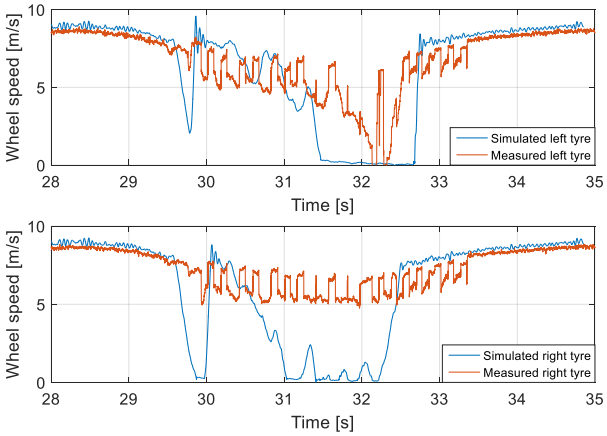

Figure 67: Wheel speeds comparison between simulated and measured results

The comparison of tyre forces, namely longitudinal and lateral forces, between the simulated and experimental results, are shown in Figure 68 and Figure 69.

Figure 68 shows the comparison between the vertical forces of the MSC ADAMS model and the actual test. This figure shows that the simulated model experiences a larger vertical force than the actual model, which cause the tyres to lock quicker. This is why the simulated braking force of the tyres shown in Figure 69 are larger in magnitude. This difference could be due to some discrepancy with the calibration of the WFT's, as well as a difference in the static position of each suspension setup.

There is some correlation that is evident with the brake forces, as the first three peaks of the left wheel match up quite closely between 30 and 30.5 seconds.

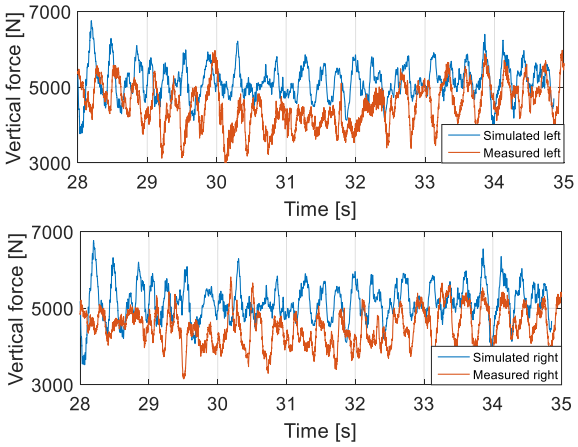

Figure 68: Vertical force comparison between simulated and measured results

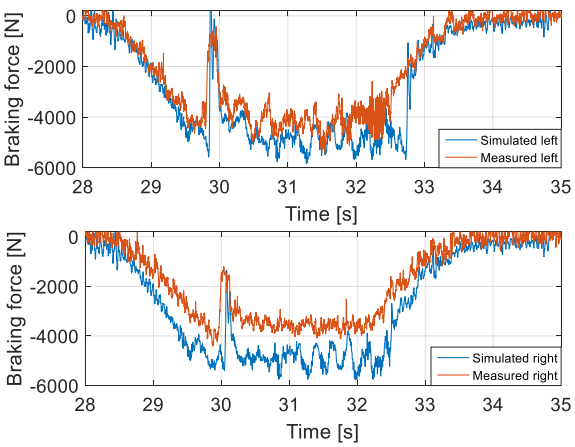

Figure 69: Braking force comparison between simulated and measured results

5.3. Belgian paving ABS test

The measured results on Belgian paving reflect the same occurrences of irregular wheel speeds, as seen with the smooth terrain tests. This test was done at a speed of $20km/h$ through braking both wheels, but only allowing the right wheel to be braked on Belgian paving.

Figure 70 shows a comparison between the wheel speeds, vehicle speed and the brake phases. The wheel speeds again show a disrupted nature and it can be observed that the right wheel speeds (on rough terrain) are noisier than the left wheel speeds (on smooth terrain). This shows the direct impact that rough terrain has on the measurement of wheel speed. The ABS test on Belgian paving shows that even though the right wheel was tested on the Belgian paving, the left wheel still locked. The wheel slips and accelerations in Figure 71 and Figure 72, seem acceptable considering the rough excitations from the terrain carried over from the wheel speeds. The accelerations once again do not exceed the a_{min}threshold.

The brake pressures in Figure 73 again show the inability of the brake system to dump pressure after three ABS consecutive cycles (after 25 seconds). When observing the pressures, it is evident that the right wheel does not lock because of the terrain roughness, rather than a result of the ABS control.

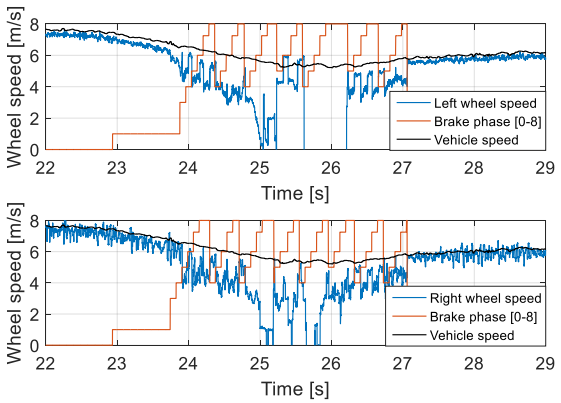

Figure 70: Wheel speeds on Belgian paving

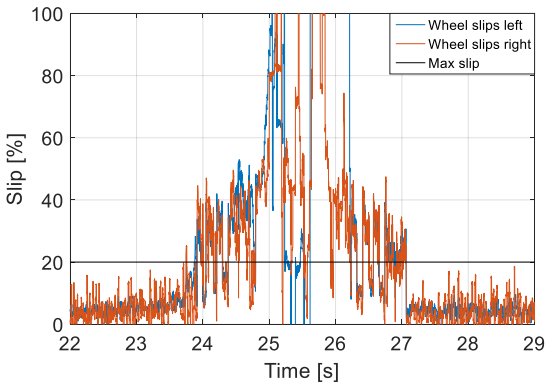

Figure 71: Wheel slip on Belgian paving

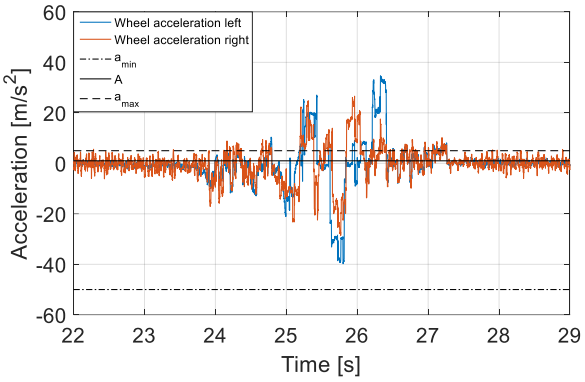

Figure 72: Wheel accelerations on Belgian paving

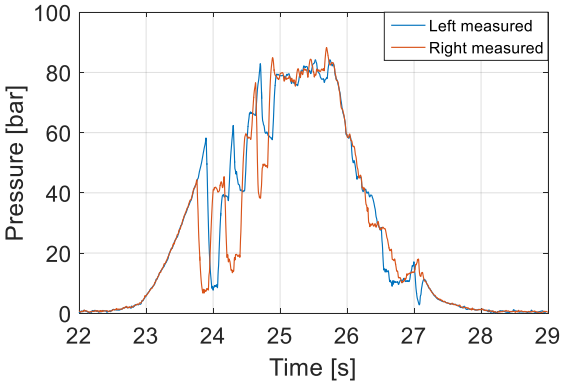

Figure 73: Brake pressures on Belgian paving

The encoder measurements from the WFT's are compared to the wheel speeds in Figure 74. There is a close correlation between these recorded variables for both wheels, except for the irregular spike in the left wheel's speed after 25 seconds.

The tyre vertical and braking forces are shown in Figure 75. The vertical force on the right tyre fluctuated much more than the left tyre, due to the rough surface of the Belgian paving. The vertical load also directly affects the braking force on the right tyre. Such an instance can be observed at 25.5 seconds, whereas the vertical force decreases, so does the braking force. This variation of vertical force could be one of the causes that kept the right wheel from locking.

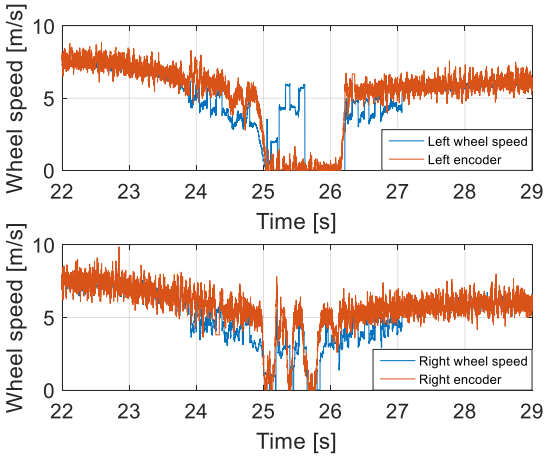

Figure 74: Wheel speeds versus encoder measurements on Belgian paving

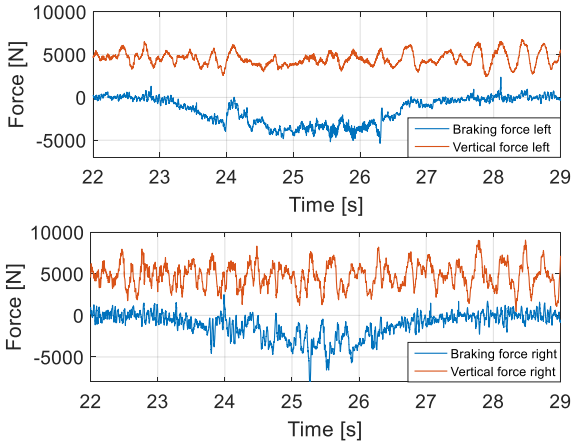

Figure 75: Tyre forces on Belgian terrain

5.4. Validation of ABS Belgian paving results

The simulated ABS tests were done at the same vehicle speed and the same brake pressures that was measured during the experimental test. The exact positioning of the model on the 3D road surface was different to that of the experimental test.

The simulated wheel speeds are compared to the measured speeds in Figure 76. It can be seen that the simulated left wheel speeds follow some aspects of the trend seen in the measured data, for the left wheel that is on smooth terrain. There are relatively good correlations between the speeds, considering that the right wheel speeds were measured on different positions on the Belgian paving.

The simulated right wheel shows wheel oscillations that have the same nature of the measured wheel speeds. This occurrence again substantiates the cause of the wheel speed jumps seen in the measured data.

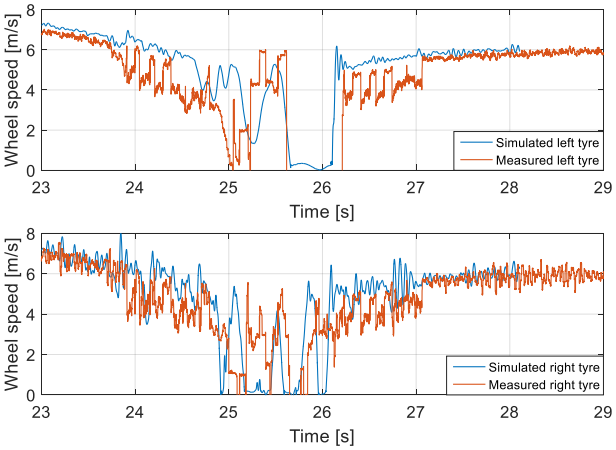

Figure 76: Wheel speeds comparison between simulated and measured results

The vertical and braking forces for the validation of the ABS tests are shown in Figure 77 and Figure 78. As mentioned before, a comparison between the wheel speeds cannot be fully completed as the potion on the Belgian paving, where the ABS tests were performed, are different from the simulations. Both figures show that the simulations have greater magnitudes in both vertical and braking forces. This could once again be caused due to the loading discrepancies of the trailer, as well as the discrepancy of the simulated brake pressure.

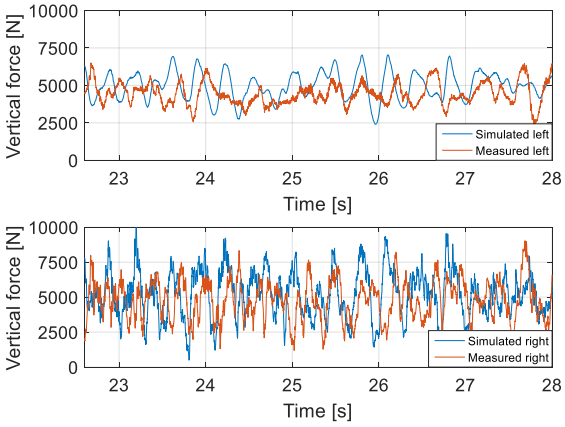

Figure 77: Vertical force comparison between simulated and measured results

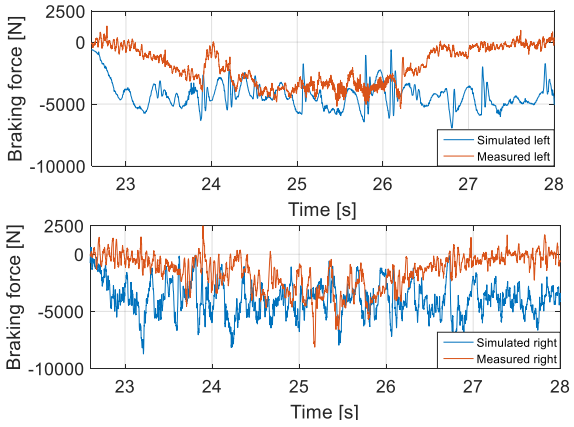

Figure 78: Braking force comparison between simulated and measured results

5.5. ABS simulations with trailer

ABS brake test simulations were also performed by using the same test vehicle speeds that were measured with the experimental ABS tests, whilst the ABS algorithm was allowed to control the brake pressure of the model. These tests show that independent ABS investigations using only the ADAMS model, are also possible and feasible.

5.5.1. ABS on smooth terrain simulations

It can be noted, that with a more accurate wheel speed (obtained from Simulink), the ABS algorithm is able to successfully prevent the wheel from locking up (Figure 79). There are instances however where the wheels are close to lock-up beyond the s_{max} threshold shown in Figure 80. It can be seen that phase 4 is skipped in some instances, due to the minimum acceleration not decreasing lower than the a_{min} threshold.

The magnitude of the simulated wheel accelerations are higher than those measured during the ABS test shown in Figure 81. It is noticed that the a_{min} threshold is still not reached, suggesting that it could be set too low for the specific trailer setup, as the wheels are only loaded with one drum, effectively half the weight that a rear Land Rover tyre should typically experience.

The expected response in the brake pressures can be seen in Figure 82, which shows continuous cycling of the brake pressures.

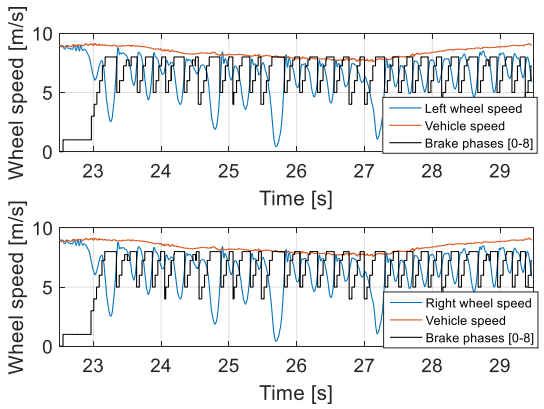

Figure 79: Wheel speeds on smooth terrain

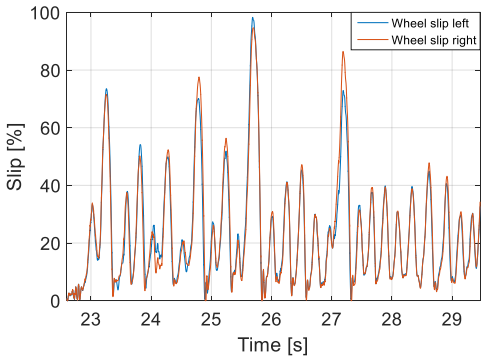

Figure 80: Wheel slips on smooth terrain

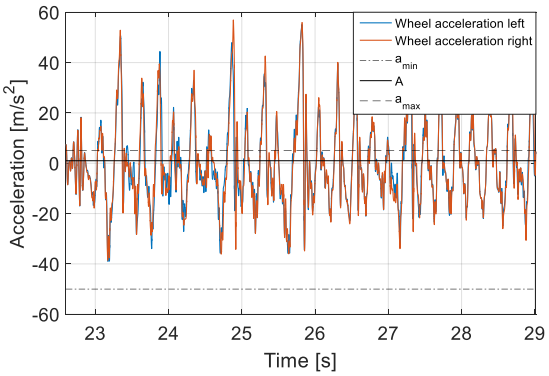

Figure 81: Wheel accelerations on smooth terrain

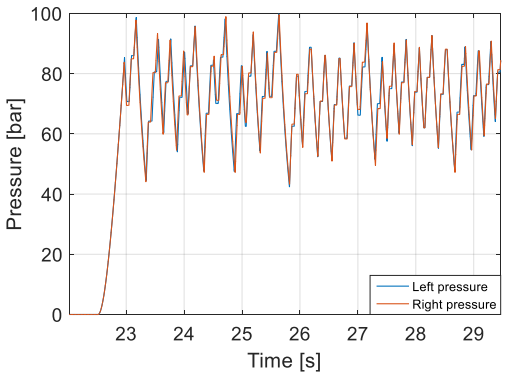

Figure 82: Brake pressures on smooth terrain

The tyre forces are shown in Figure 83 and Figure 84. It can clearly be seen, that when the vertical force increases, the braking force increases, at just before 25 seconds for both tyres.

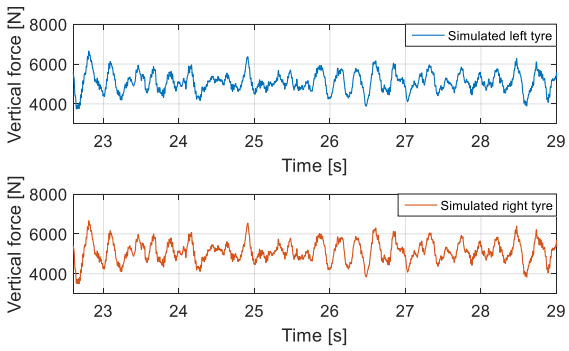

Figure 83: Vertical force smooth terrain simulation

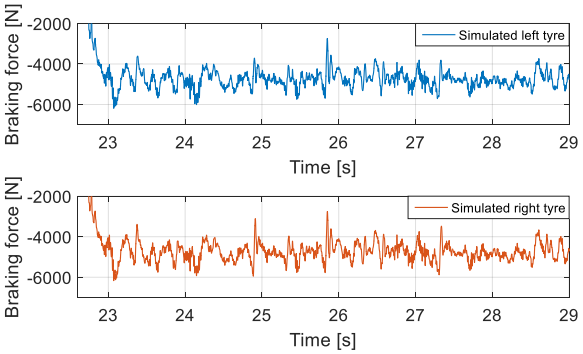

Figure 84: Braking force smooth terrain simulation

5.5.2. ABS on Belgian paving simulations

The simulations for ABS on Belgian paving show that the wheels locked up. The cause of this could be attributed to a multiple factors and is precisely the motivation behind the trailer being built.

The factors include fluctuating vertical forces on the tyres, fluctuation of friction due to terrain roughness, and fluctuating wheel speeds. In Figure 85, it is evident that substantially more wheel oscillations occur during the dumping of pressure, when the wheel speeds are increased after being locked.

The wheel speeds oscillations also cause the wheel slips to oscillate, where the s_{max} threshold is exceeded, but the wheels aren't about to be locked (refer to occurrences at 24 seconds and just after 26 seconds in Figure 86).

The wheel accelerations are much higher in magnitudes than those measured experimentally. In this case the a_{min} threshold was reached (Figure 87).

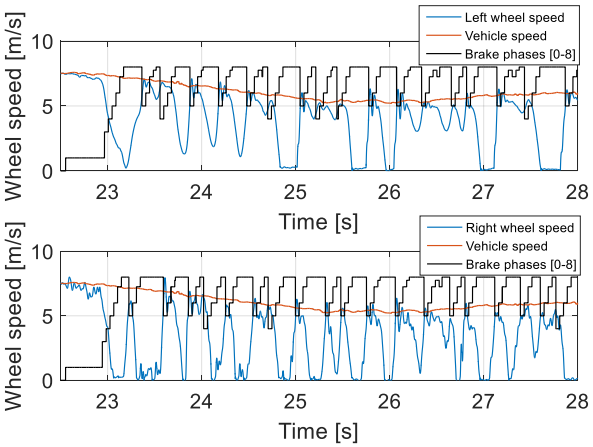

Figure 85: Wheel speeds on Belgian paving

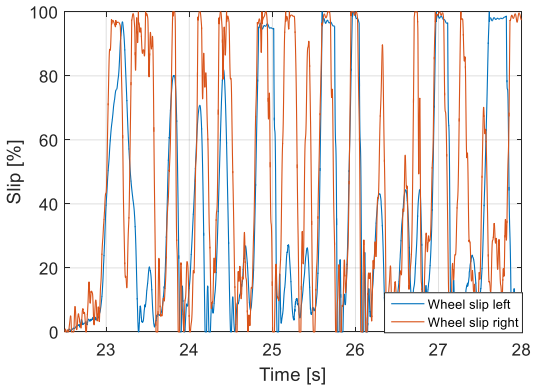

Figure 86: Wheel slips on Belgian paving

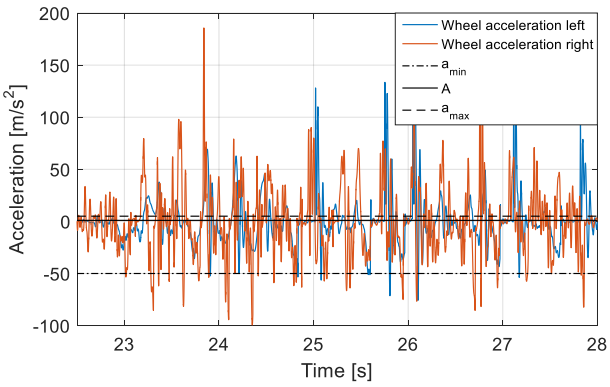

Figure 87: Wheel accelerations on Belgian paving

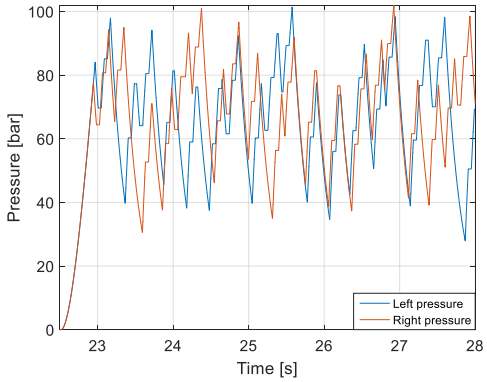

Figure 88: Brake pressures on Belgian paving

Specifically viewing at 26 and 27 seconds in Figure 89 and Figure 90, the increase of vertical force on the tyres have a predominant influence on wheel lock, causing the braking force to increase in magnitude. It is due to this disturbance in braking force that the wheels suddenly lock-up. The duration of wheel lock is also influenced by the nature of the vertical force. If the vertical force still increases further whilst the phases are in "Dump" mode (26 and 27 seconds in Figure 85 and Figure 88), a delay could be caused in releasing the wheels from being locked. It is deduced that this is one of the many reasons why ABS control is difficult to achieve on rough terrain.

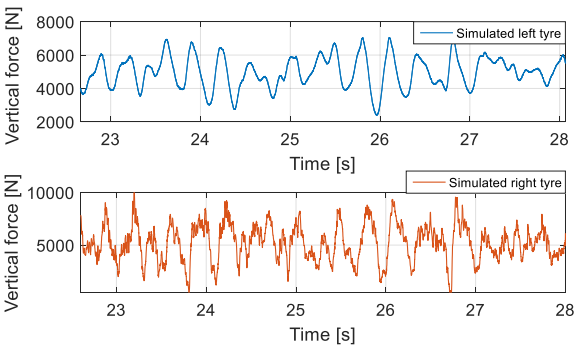

Figure 89: Vertical force Belgian paving simulation

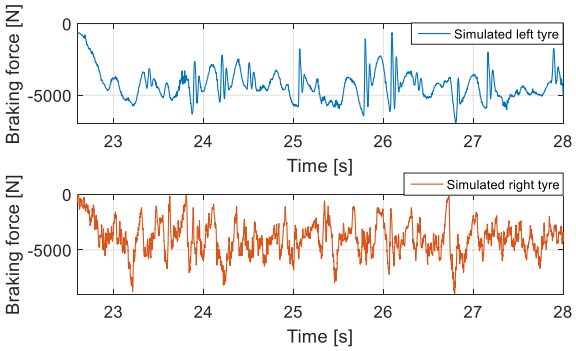

Figure 90: Braking force Belgian paving simulation

It is noteworthy that with the ABS simulations for rough terrains, the high interference from the terrain roughness and the variation in vertical load greatly influences the brake control of the wheels. It was noticed that the wheel oscillations during the release of pressure could cause the incorrect estimation of the tyre's state of slip. The assumption of a constant effective rolling radius in the calculation of slip also causes inaccuracies and this is substantially influenced by terrain roughness.

5.6. Spectral analysis of braked tyres

The spectral density of the braking force of the tyres on smooth terrain, indicates that during braking, the tyre is excited at additional frequencies close to 60Hz, seen on the left wheel. The COSIN analysis of the FTire model indicates that the tyre was excited at a frequency of 61.61Hz, which produces an in-plane mode shape.

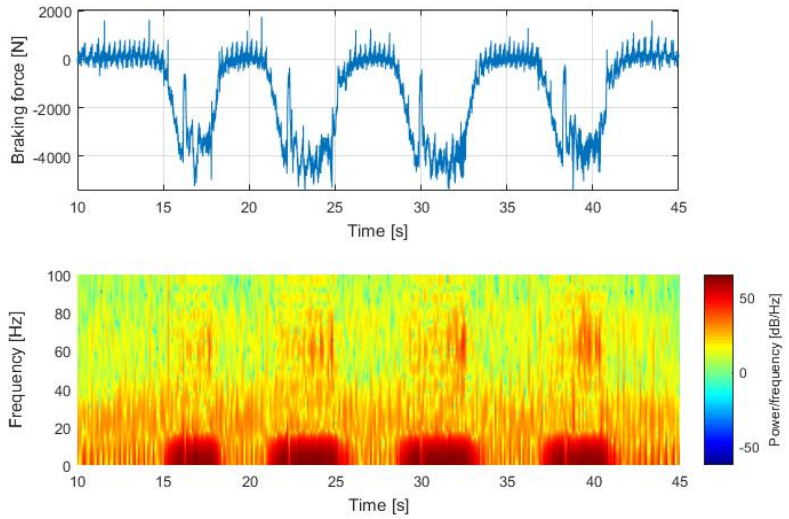

Figure 91: Left tyre on smooth terrain

By looking at the right tyre ABS performance and its spectrogram on Belgian paving, it is noticed that a larger range of frequencies are excited during braking (Figure 92). These frequencies seen in the figure were possibly also excited at mode shapes, found from COSIN that included 51.48Hz and 77.47Hz, all of which are in-plane modes. These vibrations are very close to the data found by Tuononen (Tuononen et al., 2012).

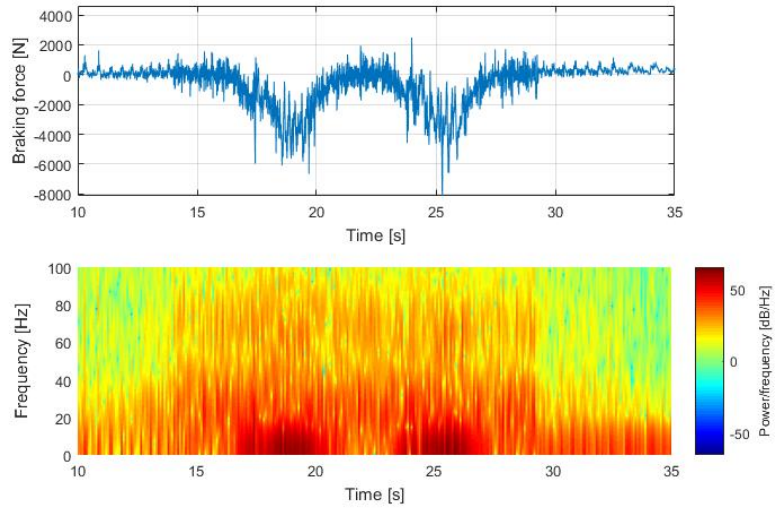

Figure 92: Right tyre on Belgian paving

5.7. Conclusion

In this chapter ABS tests were performed with the trailer on both smooth and rough terrain. The variation of wheel loads during ABS braking, especially on rough terrain, was observed. Wheel speeds fluctuated to a detrimental extent during ABS tests and the brake pressure cycling of the ABS modulator was not reliable. Simulated tests using the same speeds and brake pressures were also performed and it was found that close correlation could be found with the brake forces compared.

Simulated ABS tests were also performed and it was found that with even with a more reliable wheel speed measurement rough terrain, ABS still struggles to perform optimally. The tyre dynamics in terms of braking force was also investigated during ABS operation through performing a spectral analysis. It was found that mode shapes of the tyre were excited during ABS operation with a frequency range of 50-80Hz.

6. Conclusions and recommendations

A trailer was built, modelled and validated for the purpose of performing ABS braking tests on smooth terrain and Belgian paving. Implementing the trailer with rigid suspension was found to be of importance as this allowed the tyre-terrain interaction to be investigated through purely observing the response of the tyre, influenced only by the terrain (no suspension interferences). This also helped to validate the trailer model accurately before suspension was fitted to the trailer. It was found that, if the rigid suspension was used, ABS tests could only be performed to maximum a speed of $7km/h$, above which the tyres started loosing ground contact and the trailer became unstable. The ABS tests were not continued using this suspension setup, however model validation was done and this concluded that the tyre model used in MSC ADAMS was sufficient for ABS braking tests. A standard suspension was then fitted to the trailer to allow for ABS tests to be performed at over rough terrain. The suspension components were to be characterised to allow for accurate modelling. An acceptable validation was achieved for the trailer, with the standard suspension setup.

ABS tests were performed using ADAMS and it was found that the variation in vertical force with ABS on Belgian paving, predominantly determines how the wheels are locked and released from a locked state, mainly due to rough terrain interference. The test data and simulations substantiate the literature found on ABS braking on rough terrain, and this study concludes that a complex connection between all input variables and parameter collectively cause inefficiencies, with using the standard Bosch algorithm for rough terrains. Relatively acceptable correlation was achieved between the tyre forces measured and those simulated, using a validated FTire tyre model in MSC ADAMS, particularly with smooth terrain simulations. Mode shapes could be captured for the braked tyres between 50-$80Hz$, by looking at the spectral analysis on the braking force measured.

The ABS tests that were performed indicated that the measurement of wheel speeds was disrupted, possibly due to wheel oscillations caused by ABS operation. The modulator used failed to consecutively dump the pressure after three ABS cycles.

Further work should include improving the model in terms of the vertical force discrepancies seen in the experimental and simulation data. The method of application of brake pressure induced into the system can also be improved. The brake pedal could possibly be controlled to supply a fixed force or initiated to pull the pedal in further, if the pressure is dumped, this allows for a constant threshold of pressure, which could possibly solve the issue with dumping pressure after the first number of ABS cycles. To help achieve this the pressure between the brake pedal and the modulator inlet can also be measured and controlled. The measurement of wheel speed should also be investigated further, particularly in the event that wheel oscillations occur, so that the occurrences can be properly captured by the measurement equipment. As the trailer is equipped with a front axle, the wheels can be steered and thus ABS can also be tested for different tyre side slip angles.

The work done in this dissertation paves the way forward into further ABS investigations on rough terrain, using a platform that focusses on and isolates the tyre-terrain interaction.

7. References

ADCOX, J., AYALEW, B., RHYNE, T., CRON, S. & KNAUFF, M. 2012. Interaction of Anti-Lock Braking System with Tire Torsional Dynamics. *Tire Science and Technology* 40**,** 171–85.

AMIRI, M. & MOAVENI, B. 2012. Vehicle Velocity Estimation based on Data fusion by Kalman Filtering for ABS. *Electrical engineering (ICEE) 2012 20th Iranian Conference*.

BECKER, C. M. & ELS, P. S. 2012. Wheel Force Transducer Measurements on a Vehicle in Transit. *Proceedings of the 12th European Regional Conference of the ISTVS*.

BECKER, C. M. & ELS, P. S. 2014. Profiling of rough terrain. *International Journal of Vehicle Design,* 64.

BHANDARI, R., PATIL, S. & SINGH, R. K. 2012. Surface prediction and control algorithms for anti-lock brake system. *Transportation Research Part C: Emerging Technologies,* 21**,** 181-195.

BOSCH, H.-R. B., HAMERSMA, H. H. & ELS, P. S. 2016. Parameterisation, validation and implementation of an all-terrain SUV FTire tyre model. *Journal of Terramechanics***,** 11–23.

BOTERO, J. C., GOBBI, M., MASTINU, G., PIAZZA, N. D. & MARTORANA, R. 2007. On the Reformulation of the ABS Logic by Sensing Forces and Moments at the Wheels. . *5th IFAC Symposium on Advances in Automotive Control, IFAC Proceedings* 40**,** 265–272.

BOTHA, T. R. & ELS, P. S. 2015. Digital image correlation techniques for measuring tyre–road interface parameters: Part 2 – Longitudinal tyre slip ratio measurement. *Journal of Terramechanics,* 61**,** 101–112.

BUDYNAS, R. G. & NISBETT, J. K. 2011. *Shigley's Mechanical Engineering Design*, McGraw-Hill.

BURCKHARDT, M. & REIMPELL, J. 1993. Fahrwerktechnik, Radschlupf-Regelsysteme, Vogel.

DAID, A. & KIENCKE, U. 1995. Estimation of Vehicle Speed Fuzzy Estimation in Comparison with Kalman Filtering. *IEEE*.

DAY, T. D. & ROBERTS, S. G. 2002. A simulation model for vehicle braking systmes fitted with ABS. *SAE Technical Paper*

DSPACE. 2016. *dSPACE* [Online]. Available: https://www.dspace.com/en/inc/home/products/hw/micautob.cfm [Accessed 2016].

DUNKERMOTOREN GMBH 2015. BG75 PI Instruction manual,;.

FORKENBROCK, G., FLICK, M. & GARROT, W. R. 1999. A Comprehensive Light Vehicle Antilock Brake System Test Track Performance Evalaution. *SAE Technical Paper*.

FU, T. 2000. Modeling and performance analysis of ABS systems with nonlinear control. *Master's thesis of Applied Science Concordia University*.

GILLESPIE, T. D. 1992. *Fundamentals of Vehicle Dynamics*, Society of Automotive Engineers.

GUO, J., JIAN, X. & LIN, G. 2014. Performance Evaluation of an Anti-Lock Braking System for Electric Vehicles with a Fuzzy Sliding Mode Controller. *Energies*.

HAMERSMA, H. A. & ELS, P. S. 2014. Improving the braking performance of a vehicle with ABS and a semi-active suspension system on a rough road. *Journal of Terramechanics,* 56**,** 91-101.

HAMERSMA, H. A. & ELS, P. S. 2017. ABS performance evaluation taking braking, stability and steerability into account. *International Journal of Vehicle Systems Modelling and Testing,* 12**,** 262-283.

HARIFI, A., AGHAGOLZADEH, A., ALIZADEH, G. & SADEGHI, M. 2008. Designing a sliding mode controller for slip control of antilock brake systems. *Transportation Research Part C 16*, 731–741.

INTERNATIONAL ORGANIZATION FOR STANDARDIZATION 1995. ISO 8608: Mechanical Vibration-Road Surface Profiles-Reporting of Measured Data. *ISO 8608*.

IVANOV, V., SAVITSKI. D., AUGSBURG. K., BARBER, P., KNAUDER, B. & ZEHETNER, J. 2015. Wheel slip control for all-wheel drive electric vehicle with compensation of road disturbances. *Journal of Terramechanics*, 1–10.

JIANG, F. & GAO, Z. 2000. An Adaptive Nonlinear Filter Approach to Vehicle Velocity Estimation for ABS. *International Conference on Control Applications*, 490 - 495.

KINDT, P., SAS, P. & DESMET, W. 2009. Measurement and analysis of rolling tire vibrations. *Optics and Lasers in Engineering,* 47, 443-453.

KOBAYASHI, K., CHEOK, K. C. & WATANABE, K. 1995. Estimation of Absolute Vehicle Speed using Fuzzy Logic Rule-Based Kalman Filter. *American Control Conference Seattle*.

KOIZUMI, T., TSUJIUCHI, N., MATSUBARA, M. & NAKAMURA, F. 2010. Vibration Analysis of Rolling Tire based on Thin Cylindrical Shell Theory. *Proceedings of ISMA 2010*, 4003–4013.

LEE, T. K. & KIM, B. S. 2008. Vibration analysis of automobile tire due to bump impact. *Applied Acoustics* 69, 473–478.

LIU , G., ZHANG, Q., WANG, Y. & ZHOU, T. 2004. An investigation of Digital filter Technology on ABS wheel speed signal. *Information Acquisition Proceedings*.

MARIAN, V., LUMINITA, S. M. & SORIN, V. 2009. The Influence of Forced Steering Vibrations on a Wheel and Dynamic Effect of a Wheel with ABS Braking on Undulated Road II. *The 3rd International Conference on Computational Mechanics and Virtual Engineering", Brasov, Romania, October 29–30*.

MERIAM, J. L. & KRAIGE, L. G. 2007. *Engineering mechanics dynamics*, John Wiley and sons.

PARK, J., JEONG, H., JANG, I. G. & HWANG, S.-U. 2015. Torque Distribution Algorithm for an Independently Driven Electric Vehicle Using a Fuzzy Control Method. *Energies*.

PAUWELUSSEN, J. P. 2015. *Essentials of Vehicle Dynamics*, Elsevier.

PAUWELUSSEN, J. P., GOOTJES, L., SCHRÖDER, C., KÖHNE, K. U., JANSEN, S. & SCHMEITZ, A. 2003. Full vehicle ABS braking using the SWIFT rigid ring tyre model. . *Control Engineering Practice 11(2)*, 199–207.

PENNY, W. C. W., ; & ELS, P. S. 2016. The test and simulation of ABS on rough, non-deformable terrains;. *Journal of Terramechanics,* 67, 1–10.

POURSAMAD, A. 2009. Adaptive feedback linearization control of antilock braking systems using neural networks. *Mechatronics,* 19.

RACELOGIC LIMITED 2011. VBOX III 100Hz GPS Data Logger User Guide.

ROVER GROUP LIMITED 1996. Workshop manual Defender 300Tdi.

SAE STANDARD 1992. Anti-Lock Brake System Review. *SAE J 2246*.

SIVARAMAKRISHNAN, S., SINGH, K. & LEE, P. 2015. Experimental Investigation of the Influence of Tire Design Parameters on Anti-lock Braking System (ABS) Performance *SAE Technical Paper*.

SUBBULAKSHMI, K. 2014. Antilock-Braking System Using Fuzzy Logic. *Middle-East Journal of Scientific Research,* 20 1306-1310.

TEXAS INSTRUMENTS INCORPORATED 2013. LM1815 Adaptive Variable Reluctance Sensor Amplifier.

TSUJIUCHI, N., KOIZUMI, T., TAMAKI, R. & SHIMA, I. 2004. An Investigation of Rolling Tire Vibration Caused by Road Roughness. *Conference on Structural Dynamics*.

TUONONEN, A., HARTIKAINEN, L., PETRY, F. & WESTERMANN, S. 2012. Modeling tire vibrations in ABS-braking. *Tag des Fahrwerks*.

UYS, P. E., ELS, P. S., THORESSON, M. J., VOIG, K. G. & COMBRINCK, W. C. 2006. Experimental Determination of Moments of Inertia for an Off-Road Vehicle in a Regular Engineering Laboratory. . *International Journal of Mechanical Engineering Education 34/4***,** 291–314.

WU, M.-C. & SHIH, M.-C. 2003. Simulated and experimental study of hydraulic anti-lock braking system using sliding-mode PWM control. *Mechatronics,* 13**,** 331-351.

ZEGELAAR, P. W. A. 1998. The dynamic response of tyre to brake torque variations and road unevennesses. . *Ph.D. thesis, Delft University of Technology, The Netherlands*.

ZETTLEX 2018. IncOder Product Guide Midi Range Inductive Angle Encoders.

ZHENG, T., WANG, L. & MA, F. 2011. Research on road identification method in Anti-lock Braking System. *Procedia Engineering,* 15**,** 194-198.

ŽURAULIS, V., LEVULYTĖ, L. & SOKOLOVSKIJ, E. 2014. The impact of road roughness on the duration of contact between a vehicle wheel and road surface. . *Transport. Vilnius: Technika***,** 431-439.